Flow boiling of carbon dioxide: heat transfer for smooth and enhanced geometries and effect of oil. State of the art review

R. Mastrullo, A.W. Mauro*, L. Viscito

*Department of Industrial Engineering, Università degli studi di Napoli - Federico II, P.le Tecchio 80, 80125, Naples (Italy) - *email: alfonsowilliam.mauro@unina.it*

N.B.: This is the PREPRINT (submitted) version of this article. The final, published version of the article can be found at: https://doi.org/10.1016/j.ijrefrig.2019.08.028

Abstract

This paper presents a state-of-the-art review on flow boiling of carbon dioxide, including experimental studies and prediction methods for smooth and enhanced tubes, with pure CO_2 and CO_2/lubricant mixtures. Specifically, 5223 heat transfer coefficient data with pure CO_2 in smooth tubes were collected, and the effect of the operating conditions is discussed. The experimental Nusselts are then compared to pure nucleative and convective heat transfer, once data are sorted according to their corresponding flow pattern.

Additional 883 CO_2 data points in microfin tubes and 1184 experimental heat transfer coefficients in smooth tubes with CO_2/oil mixture are also collected, and the influence of the microfin structure and of the oil presence on the heat transfer mechanism is analyzed.

Finally, specific carbon dioxide prediction methods for two-phase heat transfer coefficient developed in smooth, enhanced tubes and with oil/CO_2 mixtures are implemented and compared with the experimental data, providing a comprehensive statistical analysis.

Keywords: CO_2; review; flow boiling heat transfer; enhanced tubes; heat transfer with oil; prediction methods.

Highlights

1) Collection of boiling data for pure CO_2 and with CO_2/lubricant mixtures.
2) Effect of operating conditions and oil presence on the heat transfer analyzed.
3) Data in smooth tubes sorted and analyzed according to their flow pattern.
4) Experimental data compared to only-convective and only-nucleative heat transfer.
5) Assessment of methods developed for flow boiling of carbon dioxide.

Contents

Nomenclature **3**
1. Introduction **5**
1.1 Background and CO_2 properties 5
1.2 Possible applications and drawbacks 6
1.3 Review outline 7
2. Experimental database for smooth tubes **7**
2.1 Recurring trends for macro and micro-channels 12
3. Assessment of predictive methods for smooth tubes **17**
3.1 Nucleate and convective boiling contributions 17
3.2 Assessment of correlations for smooth tubes 23
4. Boiling of CO_2 in enhanced surfaces and with the presence of oil **32**
4.1 Experimental database for microfin tubes 32
4.2 Heat transfer for CO_2/oil mixtures in smooth tubes 35
5. Assessment of prediction methods for enhanced surfaces and oil effect **38**
5.1 Nucleate and convective boiling contributions 38
5.2 Assessment of methods: enhanced tubes 40
5.3 Assessment of methods: oil effect 42
6. Conclusions **47**
Acknowledgements **48**
References **49**

Nomenclature

Roman

c_p	specific heat at constant pressure	[J kg^{-1} K^{-1}]
d	tube internal (equivalent) diameter	[m]
D_{eq}	equivalent diameter (for annular flow)	[m]
E	convective boiling enhancement factor	[-]
G	mass flux	[kg m^{-2} s^{-1}]
g	acceleration of gravity	[m s^{-2}]
h	heat transfer coefficient	[W m^{-2} K^{-1}]
H_{fin}	fin height	[m]
i_{LV}	latent heat	[J kg^{-1} K^{-1}]
J	superficial velocity	[m s^{-1}]
M	molecular mass	[kg kmol^{-1}]
q	heat flux	[W m^{-2}]
P	pressure	[Pa]
S	nucleate boiling suppression factor	[-]
T	temperature	[°C]
u	velocity	[m s^{-1}]
x	vapor quality	[-]

Greek

α	void fraction	[-]
λ	thermal conductivity	[W m^{-1} K^{-1}]
δ	liquid film thickness	[m]
μ	viscosity	[Pa s]
ρ	density	[kg m^{-3}]
σ	surface tension	[N m^{-1}]
θ_{dry}	dry angle	[rad]
ω_0	nominal oil mass fraction	[-]
ψ	percentage of data points falling into a ±30% error band	[%]
χ	percentage of data points falling into a ±50% error band	[%]

Non-dimensional numbers and statistical parameters

Bo	Boiling number	$\frac{q}{G \cdot i_{LV}}$
Bd	Bond number	$\frac{g(\rho_L - \rho_V)d^2}{\sigma}$
Co	Confinement number	$\frac{1}{d}\sqrt{\frac{\sigma}{g(\rho_L - \rho_V)}}$
Fr	Froude number	$\frac{u}{\sqrt{gd}}$
Nu	Nusselt number	$\frac{hd}{\lambda}$
Pr	Prandtl number	$\frac{\mu}{c_p \lambda}$
Re	Reynolds number	$\frac{\rho \cdot u \cdot d}{\mu}$
We	Weber number	$\frac{G^2 d}{\rho \cdot \sigma}$
X_{tt}	Martinelli parameter	$\left(\frac{1-x}{x}\right)^{0.9}\left(\frac{\rho_V}{\rho_L}\right)^{0.5}\left(\frac{\mu_L}{\mu_V}\right)^{0.1}$
|η|	Mean Absolute Error (MAE)	$\frac{1}{n}\sum_i \left\|\frac{h_{pred} - h_{exp}}{h_{exp}}\right\|$

η	Mean Relative Error (MRE)	$\frac{1}{n}\sum_i \frac{h_{pred}-h_{exp}}{h_{exp}}$

Subscripts

cb	convective boiling
cr	critical
exp	experimental
L	liquid
LO	liquid only
m	related to the oil/CO_2 mixture
nb	nucleate boiling
oil	lubricant
pred	predicted
red	reduced
sat	saturation
V	vapor
VO	vapor only
wet	wet portion

1. Introduction

1.1 Background and CO_2 properties

The use of carbon dioxide (CO_2 or R744 according to the ASHRAE classification) as refrigerant goes back to the earliest era of the vapor compression cycles, starting from the last decades of the 19th century. As reviewed by Kim et al. [1], the first CO_2 system was fabricated by the American Thaddeus S.C. Lowe in the late 1860s [2], even if he did not further develop his idea [3]. Later on, in 1881, Carl Linde built the first European vapor compression cycle employing carbon dioxide [4]. During the first decades of the 20th century, with improving technology, CO_2 was widely used as working fluid in air conditioning and stationary refrigeration systems as well as in marine applications, before being suddenly phased-out with the upcoming synthetic CFCs, which granted lower operating pressures and lower compressor discharge temperatures. Only in recent times, with the increasing concern for the anthropological global warming, carbon dioxide and other natural fluids are receiving a renewed interest as alternative working fluids. As suggested by Lorentzen [5], by excluding air and water, CO_2 is the refrigerant coming closest to the ideal of harmlessness to the environment. As regards its safety characteristics, it is non-toxic (a maximum acceptable concentration to avoid physiological effects is about 4-5% in volume [1]) and incombustible. Its accidental release in the liquid form will either evaporate or become solid in the form of snow that can be easily removed or left to sublimate, being therefore easier to manage than any other halocarbon plant [5].

Having a relative low critical temperature of 31.1 °C, CO_2 evaporates at much higher reduced pressures (0.43 at 0 °C) than other halogenated refrigerants (0.07 at 0 °C for R134a), thus showing peculiar thermodynamic and transport properties, for which the available boiling heat transfer prediction methods could not be sufficiently effective. Firstly, CO_2 presents the highest vapor density and vapor-to-liquid density ratio when compared to halocarbons and hydrocarbons [6], providing both an increased volumetric refrigeration capacity and smaller differences between the liquid and the vapor phase velocities, with less interface shear and a more homogeneous two-phase flow behavior than other fluids [7]. Secondly, the very low liquid viscosity contributes to limited pressure drop for boiling carbon dioxide and a surface tension lower by one order of magnitude leads from one side to destabilize the liquid surface, with increased droplet formation and entrainment, possibly causing a premature onset of dryout [7]. On the other hand, reduced surface tension tends to require lower superheat for bubble nucleation and bubble growth, thus increasing the heat transfer efficiency. As a summary, the heat transfer coefficients of boiling CO_2 are typically 2-3 times greater than those of conventional refrigerants when used at the same operating

conditions, while the pressure drop is considerably smaller and can often be neglected [8]. For this reason, the present review deals only with heat transfer topics and pressure drop is instead not addressed.

1.2 Possible applications and drawbacks

Its good thermodynamic and transport characteristics make carbon dioxide an interesting alternative refrigerant to R404A for several low-temperature applications, such as commercial refrigeration systems [9] [10] [11], cascade cycles [12] [13], and also transcritical ejector plants [14] [15] [16]. However, the very high carbon dioxide operating pressure (up to 120 bar in transcritical cycles against a typical maximum value of 20 bar for R404 systems) represents one of the drawbacks of its use, and often requires a complete re-design of components and materials. According to the thin-walled pressure vessel theory, with a gauge pressure of 20 bar for a 6 mm internal diameter tube, copper can be easily employed with a reasonable thickness of 0.50 mm, as shown in Figure 1a. By using CO_2 at 120 bar in the same diameter tube, instead, other materials such as reinforced K65 copper or stainless steels are typically considered, thanks to their higher yield stress, whereas copper would require unrealistic thicknesses. The use of lower thermal conductivity metals may in turn penalize the overall conductance UA, especially in case of fin and tube type heat exchangers, due to an increased fin pitch for manufacturing demands, and also the simultaneous increase of the wall thermal resistance and the reduction of the surface efficiency η_{sur}. Figure 1b shows the global conductance of a fin and tube (6 mm inner diameter and 0.50 mm thickness) evaporator with 10 tubes per row, 4 rows, and a length of 1.0 m, either for CO_2 (steel tubes and aluminum fins) or R404A (copper tubes and aluminum fins) as a function of the refrigerant side heat transfer coefficient. Two different total-over-internal heat transfer surface ratios of 100 and 80 are considered for the two fluids, respectively, to take into account the fin pitch differences. The air-side heat transfer coefficient h_e, the surface efficiency η_{sur} and the UA expression are all taken and calculated from the work of Wang and Chi [17] [18]. It is highlighted that for typical two-phase heat transfer coefficient values included in a range of 2.0 and 10.0 kW/m^{2}K, the use of different materials to cope with the higher CO_2 system pressures leads to a non-negligible penalization on the global conductance UA, that should be carefully taken into account during the design process.

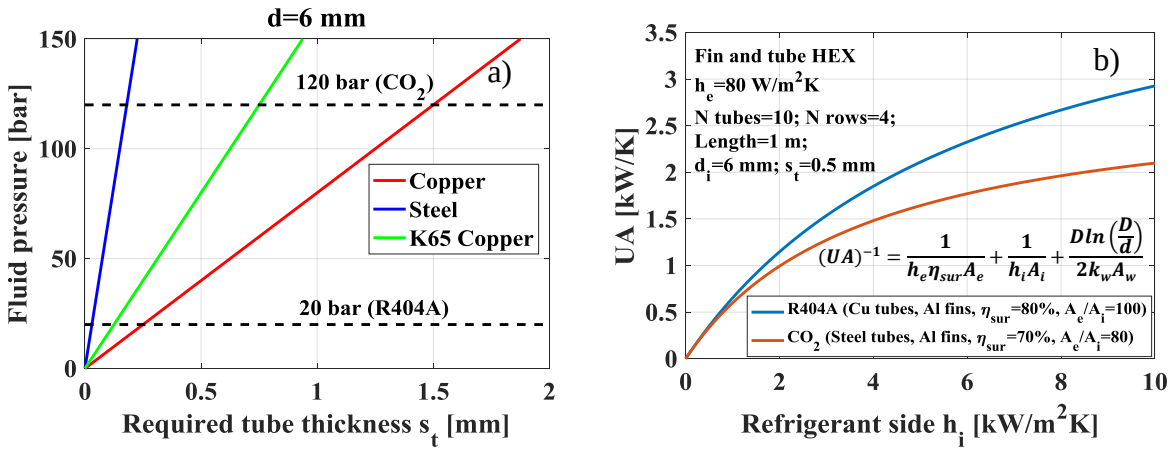

Figure 1 (a) Required thickness for a cylindrical pressure vessel having an internal diameter of 6.0 mm, for three different materials used for heat exchangers manufacturing, according to: $s_t = \frac{pd\Gamma}{2\sigma_y}$ (with σ_y as yield stress and Γ=2 as factor of safety). (b) Global conductance in a fin and tube HEX by using either steel (for CO_2) or copper tubes (for R404A), as a function of the refrigerant side heat transfer coefficient.

1.3 Review outline

The main goal of the present work is to provide an overview of the experimental CO_2 flow boiling research studies, together with an assessment of the available correlations specifically developed for carbon dioxide, thus updating the latest state of the art by Thome and Ribatski [8] performed in 2005. Specifically, a general description and trend analyses of the databank is presented, consisting in approximately 7000 heat transfer coefficient points from more than 40 independent studies, including smooth and enhanced tubes with pure CO_2 and CO_2/oil mixtures. The convective and nucleate boiling contributions are also critically evaluated for several subsets of the database (separated for smooth tubes by flow pattern). Moreover, for each dataset, the assessment of the available heat transfer prediction methods explicitly developed for carbon dioxide is finally carried-out.

2. Experimental database for smooth tubes

The research has highlighted 37 flow boiling studies using carbon dioxide as working fluid, from 2002 until 2019, covering a wide range of operating conditions. In this section, only pure CO_2 data in smooth tubes have been isolated from those works including CO_2 mixtures with other refrigerants, oils and microfinned surfaces (that will be instead the topic of the following section), by collecting a total amount of 5223 heat transfer coefficient data. The experiments have been

performed for mass fluxes from 40 to 1500 kg/m^{2}s, saturation temperatures from -40 to +25 °C, heat fluxes from 0.5 to 60 kW/m^2, tube diameters from 0.51 mm to 14 mm and different geometrical configurations (single/multi-channels, circular/rectangular pipes). All the experiments have been conducted in horizontal tubes. The whole database is shown in Table 1 and has been split for the readers' convenience in macro and micro-channel studies. Some macro-to-micro scale transition criteria are based on the tube diameter, as for the method of Mehendale et al. [19] and of Kandlikar and Grande [20], in which 6 mm and 3 mm are respectively set as threshold between conventional and compact tubes. In the present study, the experimental data are denominated as macro and micro scale according to the method proposed by Kew and Cornwell [21], which is an approximate physical criterion based on the confinement effect of a bubble within a channel. As stated by the authors, for Confinement numbers Co>0.5 (defined in nomenclature), the macroscopic laws are not suitable to predicts flow pattern transitions and heat transfer coefficients.

Figure 2 shows the threshold diameter from macro to mini-scale according to the three mentioned criteria as a function of the saturation temperature, including also the experimental points from the smooth tube database. It is worth noting that, according to the method of Kew and Cornwell, the transition diameter changes with saturation temperature, passing from approximately 2.5 mm at -50 °C up to 0.35 mm in case of +30 °C. With this criterion, most of the collected data points (55%) fall within the macro-scale region.

Among the macro-channel studies, Yun et al. [22] investigated heat transfer and dryout characteristics of carbon dioxide in a horizontal tube with an inner diameter of 6.0 mm, a wall thickness of 1.0 mm and a heated length of 1.4 m. They found that dryout of CO_2 is anticipated with respect to refrigerant R134a and that the correlation of Gungor and Winterton [23] gave good prediction of boiling heat transfer coefficient data only for high mass fluxes. Later on, the same authors presented two new studies, the first dealing with boiling CO_2 in a multi-microchannel heat exchanger with rectangular tubes [24], finding that the experimental heat transfer coefficient were well predicted by the typical pool boiling correlations. Their latest work [25] presented instead new experimental data in tubes of 0.98 and 2.0 mm, focusing on the post-dryout region and proposing a correlation.

Yoon et al. [26] measured two phase heat transfer and pressure drop of evaporating carbon dioxide in a 7.53 mm tube and a length of 5 m, in which the heat flux was provided by directly applying DC current to the test tube. It was found that the heat transfer coefficient was increasing with vapor quality and with heat flux, showing a typical nucleate boiling trend, even if a quite premature dryout was observed.

Zhao and Bansal [27] studied boiling heat transfer of CO_2 at a low temperature of -30 °C in a horizontal 4.57 mm tube (at -30 °C) and observed a convective behavior, with the experimental heat transfer coefficient increasing with vapor quality up to the onset of dryout. The authors found that none of the tested correlations (including that of Yoon et al. [26] explicitly developed for CO_2) were able to satisfactorily predict their experimental data.

Choi et al. [28] [29] [30] conducted a series of experiments on boiling heat transfer of carbon dioxide in small tubes of 1.5 and 3.0 mm having a heated length of 2000 and 3000 mm, respectively. It was found that the heat transfer coefficient was higher for the lower diameter tube at the same conditions and that nucleate boiling contribution was predominant, especially at low vapor quality region, with a significant effect of the heat flux and a negligible influence of the mass velocity.

Hihara and Dang [31] provided experimental flow boiling data of carbon dioxide in pre- and post-dryout region in a 2 mm tube. They observed that the effects of the heat flux and saturation temperature were significant in the pre-dryout region, whereas mass flux was the dominating factor affecting both the onset of dryout and also the heat transfer coefficient in the post-dryout heat transfer region.

Park and Hrnjak [32] investigated two-phase heat transfer and pressure drop of CO_2 and R410A in a 6.1 mm tube at relatively low saturation temperatures of -15 °C and -30 °C. The authors found that the heat transfer coefficients for carbon dioxide were much higher than those of R410A, especially for low vapor quality ranges, attributing this behavior to the lower molecular weight and the higher reduced pressure of CO_2 that imply a higher nucleate boiling contribution. Moreover, the heat transfer coefficients of carbon dioxide showed a strong dependence only from the imposed heat flux, whereas in case of R410A the heat transfer efficiency was affected by the change of mass flux, heat flux and vapor quality.

Oh et al. [33] [34], in two different studies, experimentally evaluated the effect of operating conditions on the two-phase heat transfer coefficient of carbon dioxide among other fluids in smooth macro-tubes of 7.75 mm and 4.57 mm, respectively. In both cases, the authors found a strong influence of the heat flux, whereas the effect of vapor quality was dependent on the specific operating condition tested. Among the different correlations implemented, the flow pattern based methods of Thome and El-Hajal [35] and of Cheng et al. [36] developed for CO_2 gave the best predictions.

In their horizontal smooth tube of 6.0 mm, Mastrullo et al. [37] [38] [39] presented a series of experiments on flow boiling heat transfer of carbon dioxide and R410A exploring the effect of the reduced pressure on flow pattern transition and heat transfer coefficient. The authors verified that,

when working at the same reduced pressure, the two-phase flow structures and the heat transfer coefficient trends with vapor quality were similar for both fluids. However, they found strong difference in their absolute values, implying that nucleate boiling contribution was predominant for CO_2, whereas R410A was more affected by the convective boiling. Among the tested correlations, the CO_2 heat transfer coefficients were quite well predicted by the flow pattern based method of Cheng et al. [36].

Zhu et al. [40] presented experimental heat transfer coefficient values for CO_2/propane mixture at different mass concentrations. In case of pure carbon dioxide, the authors found a significant influence of the saturation temperature and heat flux, whereas mass flux and vapor quality caused a minor effect.

Concerning the micro-scale database, Pettersen [41] [42] performed a comprehensive experimental campaign on flow boiling of carbon dioxide in a multiport extruded tube with circular minichannels of 0.98 mm internal diameter. The results showed that nucleate boiling contribution dominated at moderate vapor quality, where the heat transfer coefficient increased with heat flux and temperature and was less affected by varying mass flux and vapor quality. Similar multi-minichannel geometries were also later on investigated by Jeong and Park [43] and Wu et al. [44].

Gasche [45] provided flow visualization and heat transfer data of flow boiling of CO_2 in a narrow rectangular channel having an equivalent diameter of 0.8 mm. The high data scattering did not permit to identify a clear dependency of the heat transfer coefficient with the mass flux and vapor quality, even if the experimental data were quite well fitted with the pool boiling correlation of Gorenflo [46].

Ducoulombier et al. [47] performed a comprehensive experimental campaign on flow boiling heat transfer of carbon dioxide in a single minichannel having an internal diameter of 0.529 mm. The authors observed both typical nucleate and convective boiling trends, depending on the operating conditions. Similar outcomes were also found in the recent studies of Linlin et al. [48] and of Liang et al. [49].

Finally, Ozawa et al. [50] [51] mostly focused on the effect of the reduced pressure on the boiling CO_2 flow patterns. Even if the experiments were performed in the narrowest tube of the present database (0.51 mm), the authors still observed stratification of the liquid phase and therefore a marked difference in the heat transfer coefficient at the upper and lower walls.

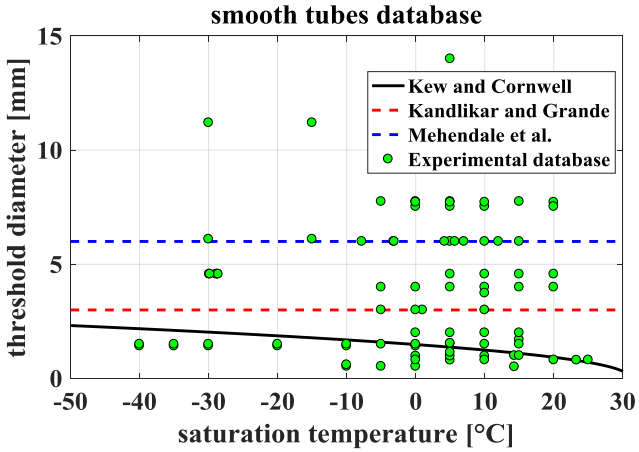

Figure 2 Transition diameter from conventional to micro-scale according to the threshold criteria of Kew and Cornwell **[21]**, Mehendale et al. **[19]** and Kandlikar and Grande **[20]** implemented for CO_2, as a function of the saturation temperature. The markers represent the collected experimental data for smooth tubes in this study.

Table 1 Experimental databank for boiling of pure CO_2 in smooth tubes. Data for macro and micro-scale are split according to the criterion of Kew and Cornwell **[21]**

Author	**Geometry***	**Internal diameter [mm]**	**Mass velocity [kg m^{-2} s^{-1}]**	**Heat flux [kW m^{-2}]**	**Saturation temperature [°C]**	**Number of points**
Macro-scale (Co<0.50)						
Yun et al. [22]	S,C,H	6	170/340	10/20	5/10	135
Yoon et al. [26]	S,C,H	7.53	318	12.5/18.6	0/20	53
Schael and Kind [52]	S,C,H	14	75/300	3/60	5	26
Cho et al. [53] [54]	S,C,H	4/7.72	212/656	6/30	-5/20	200
Zhao and Bansal [27]	S,C,H	4.57	139.5/231	12.6/19.3	-30	23
Choi et al. [28] [29] [30] [55]	S,C,H	1.5/3	250/600	10/40	-5/10	446
Hihara and Dang [31]	S,C,H	1/2	360/1440	4.5/36	5/15	189
Gao et al. [56]	S,C,H	3	380	10	10	13
Park and Hrnjak [32]	S,C,H	6.1	100/400	5/15	-30/-15	108
Oh et al. [33] [34]	S,C,H	4.57/7.75	200/900	10/40	-5/20	209
Katsuta et al. [57]	S,C,H	3	400	5/15	0/10	51
Yun and Kim [25]	S,C,H	0.98/2	360/1500	18/40	0/15	265
Mastrullo et al. [37] [58] [38] [39]	S,C,H	6	162/526	5/20.3	-7.8/12	532
Pehlivanoglu et al. [59]	S,C,H	6.1	100/400	2/15	-30/-15	84
Kim et al. [60]	S,C,H	11.2	40/200	0.5/10	-30/-15	116
Ono et al. [61]	S,C,H	3.74	190/380	10/30	10	61
Dang et al. [62]	S,C,H	2/6	360/1440	18/36	15	322
Zhu et al. [40]	S,C,H	2	200/400	5/15	0/10	76
Liang et al. [49]	S,C,H	1.5	300/600	7.5/30	-35/15	89
Micro-scale (Co>0.50)						
Pettersen et al. [41] [42]	M,C,H	0.79	190/570	5/20	0/25	103
Yun et al. [24]	M,R,H	1.08/1.54	200/400	10/20	0/10	57
Gasche [45]	S,R,H	0.8	58/235	1.8	23.3	63
Jeong and Park [43]	M,C,H	0.8	400/800	12/18	0/10	51
Ducoulombier et al. [47]	S,C,H	0.529	200/1400	10/30	-10/0	1185
Ozawa et al. [50]	S,C,H	0.51/1	500/900	30/40	14.3	113
Wu et al. [63]	S,C,H	1.42	300/600	7.5/29.8	-40/0	445
Wu et al. [44]	M,C,H	1.7	200/600	4.17/8.33	15	62
Linlin et al. [48]	S,C,H	0.6/1.5	300/600	7.5/30	-40/0	146
Overall		**0.51/11.2**	**40/1500**	**0.5/60**	**-40/+25**	**5223**
**M=multi, S=single; C=circular, R=rectangular; H=horizontal, V=vertical*						

2.1 Recurring trends for macro and micro-channels

In typical vapor compression cycle applications, carbon dioxide has a very high reduced pressure and therefore shows a peculiar flow boiling behavior with respect to other refrigerants, since the relative importance of the convective and nucleate boiling contributions are altered. Specifically, the nucleate boiling heat transfer is enhanced by means of a very low surface tension and a high vapor density, both of them contributing to trigger the bubble nucleation phenomenon with lower required wall superheats [64]. As a consequence, the two-phase heat transfer coefficients of CO_2 are generally higher than those of halogenated refrigerants, as testified by different comparison studies [24] [39] [29] [30]. However, no general conclusions can be driven from the above considerations,

and despite a higher magnitude of the nucleate boiling contribution, the carbon dioxide two-phase heat transfer coefficients might still present a typical convective behavior, depending on the tested operating conditions.

Some recurrent trends showing the effect of the mass flux on the CO_2 evaporating heat transfer coefficient are shown in Figure 3a-d, for conventional (a-b) and small-diameter tubes (c-d). From the study of Liang et al. [49] in Figure 3a (borderline between the macro and micro-scale), a typical convective behavior is observed when the imposed heat flux is relative low (7.5 kW/m^2), with an increasing heat transfer coefficient with vapor quality and mass velocity. The slope of the curves with vapor quality also increases for higher mass fluxes. The same trends can be observed at similar conditions in other macro-channel studies [32] [60] [55] [59]. When a high heat flux is imposed (Figure 3b with the study of Oh and Son [34] in a 4.57 mm tube), the effect of both mass flux and vapor quality on the local heat transfer coefficient is almost negligible. It is worth noting that a slight reduction of the dryout vapor quality is obtained with increasing mass velocity. Similar nucleate boiling-driven behaviors in macro-tubes are found in [31] [62] [37]. The same considerations can be made in case of minichannels, in which a typical convective behavior is observed in the work of Ducoulombier et al. [47] in their 0.529 mm tube (Figure 3c) as well as in [63] [48] [45]. For higher heat fluxes, the effect of the mass flux becomes negligible and slightly affects the dryout occurrence, as presented in the narrow tube of Ozawa et al. [50] (Figure 3d). In the multi-minichannel test section of Pettersen [41] [42], the heat transfer coefficient decreases with vapor quality with almost no effect of the mass flux, as also observed in the single minitube of Jeong and Park [43]. The same decreasing trend with vapor quality is found in larger tubes in case of high imposed heat fluxes in [40] and [53].

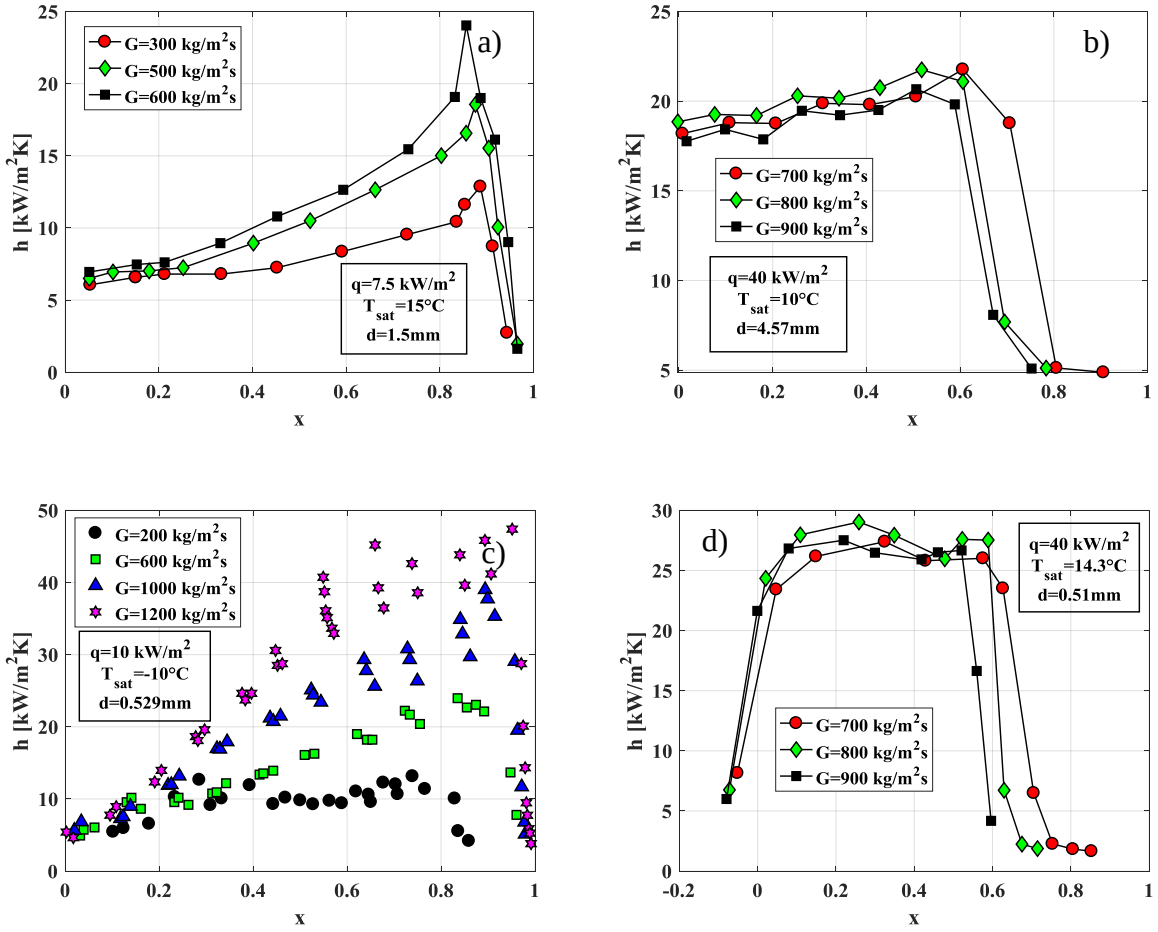

Figure 3 Effect of mass flux on CO_2 boiling heat transfer coefficient. (a) Convective behavior in macro-channels: data from Liang et al. **[49]**. (b) High imposed heat flux in macro-channels: data from Oh and Son **[34]**. (c) Convective behavior in micro-channels: data from Ducoulombier et al. **[47]**. (d) High imposed heat flux in micro-channels: data from Ozawa et al. **[50]**

The typical effects of the imposed heat flux on CO_2 boiling heat transfer coefficients are shown in Figure 4 for macro- (a-b) and microchannels (c-d). In the first case, for relatively low mass velocities, the heat transfer coefficient remains substantially the same with ongoing evaporation and is strongly affected by a change of the heat flux, as observed by Grauso et al. [39] in their 6.0 mm tubes for a saturation temperature of 7 °C and a mass flux of 200 kg/m^{2}s (Figure 4a). Similar behaviors in conventional channels are found in [33] [26] [22], with a constant or even decreasing heat transfer coefficient trends with vapor quality, that can be caused either by an anticipated dryout or by a stratification of the flow. With increasing mass velocity (see the work of Choi et al. [29] in Figure 4b), the effect of the heat flux might be confined to the low vapor quality region, where the nucleate boiling contribution is still prevailing, while typical convective trends can be observed for higher vapor qualities. Similar outcomes are found also for micro-channel studies. For the data of Wu et al. [63] in their 1.42 mm tube at G=400 kg/m^{2}s (Figure 4c), the heat flux has a significant

effect for the whole investigated vapor quality region. The change from convective to nucleate boiling driven heat transfer is also clear with increasing heat flux, as also observed by [48]. For the highest heat flux. Pure convective trends, with a negligible effect of the imposed heat flux, are shown for the microscale study of Ducoulombier et al. [47] in Figure 4d, when a high mass flux is imposed.

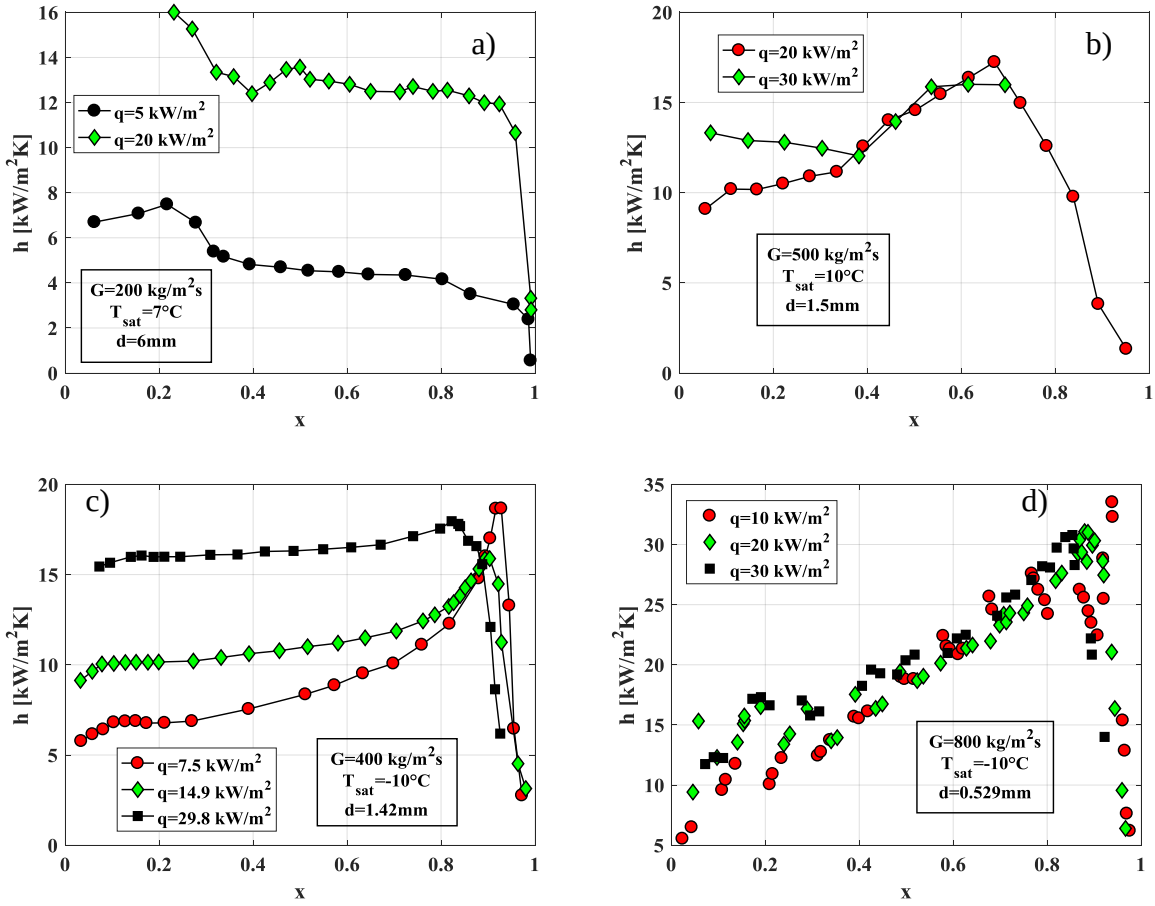

Figure 4 Effect of heat flux on CO_2 boiling heat transfer coefficient. (a) Low mass velocities in macro-channels: data from Grauso et al. **[39]**. (b) High mass velocities in macro-channels: data from Choi et al. **[29]**. (c) Low mass velocities in micro-channels: data from Wu et al. **[63]**. (d) High mass velocities in micro-channels: data from Ducoulombier et al. **[47]**

Finally, the effect of the saturation temperature can be different according to flow pattern recorded by the original authors and hence to the relative importance of the nucleate and convective boiling contributions. In case of convective-driven heat transfer, as observed in the single 0.529 mm minichannel of Ducoulombier et al. [47] and by Linlin et al. [48] in their 1.5 mm tube at 300 kg/m^{2}s and 7.5 kW/m^2 (Figure 5a), an increase of the saturation temperature leads to a reduction of the heat transfer coefficient, especially for high vapor qualities. In fact, for a higher reduced pressure, the increased density leads to a reduction of the fluid mean velocity for a fixed mass flux, thus

penalizing the convective contribution. For low vapor qualities, instead, a higher density benefits the nucleate boiling heat transfer by increasing the number of active sites [65]. This effect is particularly clear in case of nucleate boiling predominance throughout the evaporation, for high imposed heat fluxes, as shown in Figure 5b for the study of Liang et al. [49] and also in [63] and [42]. As already mentioned, the reduction of the surface tension with increasing reduced pressure enhances the boiling phenomenon, but on the other hand weakens the stability of the liquid film on the heated wall, thus possibly leading to a premature dryout, as highlighted in the horizontal 4.57 mm tube of Oh and Son [34] in Figure 5c. An earlier dryout for carbon dioxide with increasing saturation temperature was also observed by Yoon et al. [26] and Oh et al. [33].

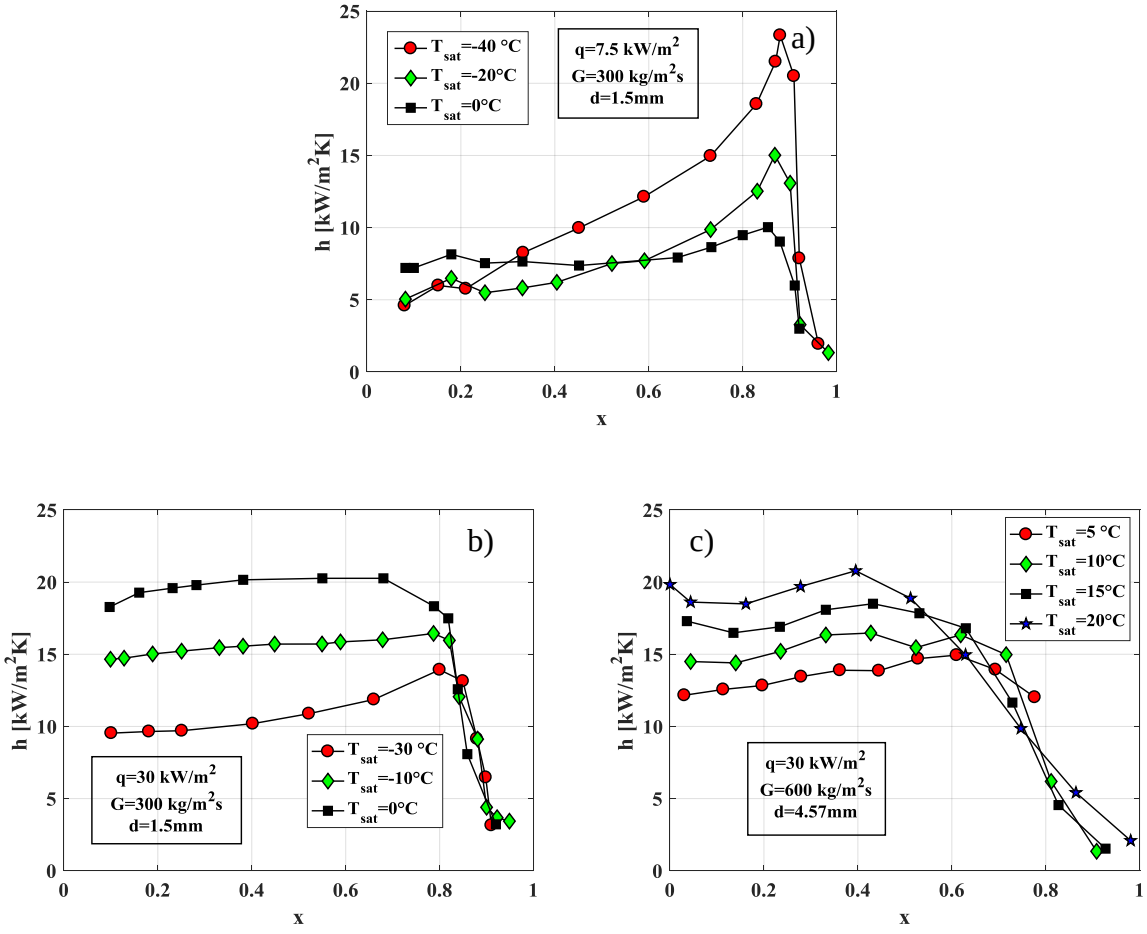

Figure 5 Effect of saturation temperature on CO_2 boiling heat transfer coefficient from different studies in micro and macro-tubes. (a) Data from Linlin et al. **[48]**. (b) Data from Liang et al. **[49]** (c) Data from Oh and Son **[34]**

3. Assessment of predictive methods for smooth tubes

3.1 Nucleate and convective boiling contributions

Figure 6a-f presents a bar chart distribution of the smooth tube database. The experimental heat transfer coefficients from all the authors have been combined (5223 points) and segregated into different categories according to their operating conditions, in terms of tube internal diameter, mass flux, saturation temperature, heat flux, Boiling number and vapor Weber number. Except for the 6.0 mm value, most of the data are obtained in smaller than 2.5 mm, with the works of Ducoulombier et al. [47] and Ozawa et al. [50] that provide alone more than 1200 data points in minichannels of 0.5 mm. Remarkable peaks for the imposed heat flux and saturation temperature distributions are respectively found at 10, 20 and 30 kW/m^2 and between -10 and +15 °C. As for the boiling and inertia contributions, 99% of the database includes Boiling numbers lower than $6 \cdot 10^{-4}$ and Weber vapor numbers lower than 3000.

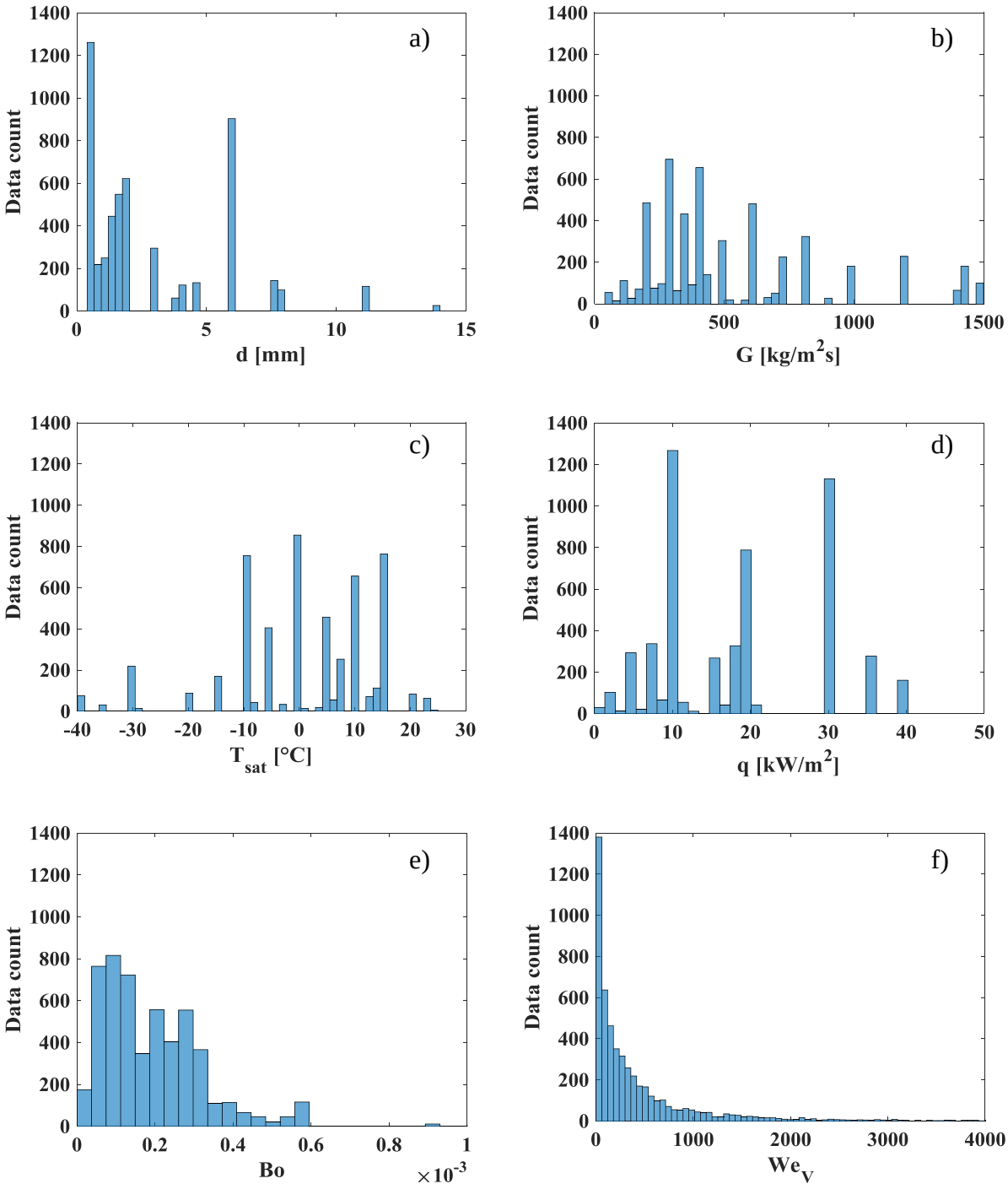

Figure 6 Distribution of data points for flow boiling of CO_2 in smooth tubes related to: (a) internal diameter; (b) mass flux; (c) saturation temperature; (d) imposed heat flux; (e) Boiling number; (f) vapor Weber number

A fair analysis of the relative importance between the nucleate and convective boiling contributions requires the knowledge of the flow regimes occurring during each experiment. However, this information is almost never provided by the original authors and therefore the collected heat transfer coefficients do not have a corresponding verified flow pattern. In this review, the flow pattern map of Cheng et al. [66], explicitly developed for carbon dioxide, is implemented for the

recognition of the flow regime related to each test. This methods allows to distinguish bubbly flow, slug+stratified wavy flow, stratified-wavy flow, stratified flow, intermittent flow, annular flow, dryout and mist flow regimes, as shown in Figure 7a presenting also the experimental liquid and vapor superficial velocities. According to the Cheng et al. [66] flow pattern map, the distribution of the flow regimes for the entire smooth tube database is shown in Figure 7b. Most of the collected data are expected to fall into the annular flow regime, with more than 2500 experimental points, followed by the mist flow regime (961), dryout (850) and intermittent flow (450). The remaining bubbly, stratified, stratified-wavy and slug flow regimes include only 450 heat transfer coefficient data.

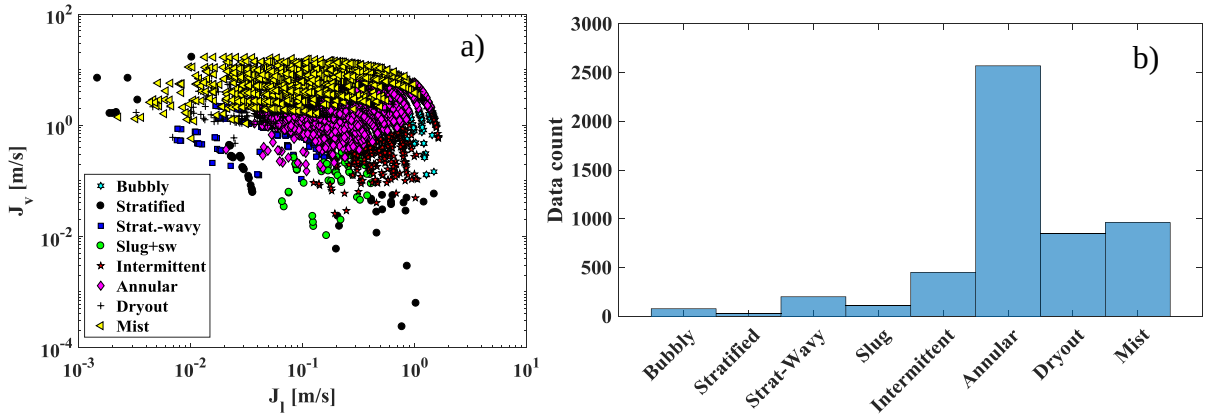

Figure 7 (a) Experimental superficial liquid and vapor velocities. Flow patterns according to Cheng et al. **[66]** model. (c) Distribution of data points related to the occurring flow patterns

As pictured from Figure 3 to Figure 5, the collected heat transfer coefficients in smooth tubes showed different trends with vapor quality and a distinct influence of the mass flux, heat flux and saturation temperature, according to their operating conditions. That is to remark that both typical nucleate boiling and convective boiling behaviors are observed during flow boiling of carbon dioxide. As first analysis, the two contributions are firstly separated to evaluate their agreement to the experimental data. Particularly, the nucleate boiling Nusselt number is calculated by using the well-known Cooper [67] pool boiling correlation, without employing any suppression factor:

$$Nu_{nb} = \frac{h_{Cooper} d}{\lambda_L} = Nu_{Cooper} = \frac{d}{\lambda_L} \cdot \left(55 P_{red}^{0.12} (-\log(P_{red}))^{-0.55} M^{-0.5} q^{0.67}\right) \quad (1)$$

As regards the convective contribution, instead, the common practice is the use of a forced convection prediction method for single phase multiplied by an enhancement factor *E* that takes into account the flow acceleration with ongoing evaporation. Here, we assume the liquid phase

distribution as a symmetric annular flow with a constant liquid film thickness δ around the heated wall, as shown in Equation (2).

$$Nu_{conv} = \frac{hD_{eq}}{\lambda_L} = a\left(\frac{\rho_L u_L D_{eq}}{\mu_L}\right)^b Pr_L^c \tag{2}$$

The equivalent diameter for the liquid annulus can be geometrically related to the liquid film thickness (Equation (3)), which is in turn a simple function of the superficial void fraction α (Equation (4)).

$$D_{eq} = \frac{4(\pi d\delta)}{\pi d + \pi(d-2\delta)} \cong 2\delta \tag{3}$$

$$\delta = \frac{d}{2}\left(1-\alpha^{0.5}\right) \tag{4}$$

The liquid phase actual velocity u_L can be expressed as a function of the liquid-only velocity (as the liquid phase would flow alone in the whole cross section) and the vapor quality and void fraction, as shown in Equation (5).

$$u_L = u_{LO}\frac{1-x}{1-\alpha} = \frac{G(1-x)}{\rho_L(1-\alpha)} \tag{5}$$

By referring the experimental Nusselt number to the tube diameter (being the liquid film thickness unknown) and substituting Equations (3), (4) and (5) in Equation (2), the convective contribution reads as Equation (6):

$$Nu_{conv,exp} = \frac{hd}{\lambda_L} = \left[a\left(\frac{Gd}{\mu_L}\right)^b Pr_L^c\right]\cdot\frac{(1-x)^b}{(1-\alpha)^b\left(1-\alpha^{0.5}\right)^{1-b}} \tag{6}$$

The first term of the third member is a typical liquid-only convection heat transfer correlation and the last term is an enhancement factor *E*. Given constants *a*, *b* and *c* as from the Dittus and Boelter [68] expression and respectively equal to 0.023, 0.8 and 0.4, the convective contribution is finally evaluated with Equation (7):

$$Nu_{conv,exp} = \frac{(1-x)^{0.8}}{(1-\alpha)^{0.8}\left(1-\alpha^{0.5}\right)^{0.2}}\cdot\left[0.023Re_{LO}^{0.8}Pr_L^{0.4}\right] = E\cdot Nu_{LO,Dittus-Boelter} \tag{7}$$

in which the void fraction α is calculated with the Steiner [69] version of the Rohuani and Axelsson [70] drift flux model.

In case of mist flow data, the experimental Nusselt numbers is computed with the vapor phase thermal conductivity, whereas the enhancement factor is not considered and the Dittus-Boelter expression takes into account the vapor properties.

The experimental Nusselt numbers are compared with both nucleate and convective Nusselt, respectively from Equations (1) and (7) in Figure 8a-f, by segregating the database according to the flow regime obtained with the Cheng et al. [66] model. In case of bubbly, slug, stratified-wavy or intermittent flow regime, the experimental Nusselt numbers are higher than the only-convection Nusselt estimated values (Figure 8a), whereas they are surprisingly well predicted by considering only the Cooper correlation for pool boiling (Figure 8b). As regards annular flow points, they are not fairly predicted with either only convection (Figure 8c) or only nucleation heat transfer (Figure 8d). For this bunch of data, a more elaborate correlation combining both contributions should instead be considered. For dryout and mist flow data, the experimental Nusselt numbers are compared only to the convective heat transfer expression, since nucleation is not likely to occur for such flow regimes. Consistently, the dryout data are generally overestimated by the convective contribution, implying that specific flow pattern based methods should be used. The remaining well predicted data are most likely to belong instead to the annular flow regime, suggesting that the annular-dryout transition criterion of Cheng et al. [66] should be modified. Mist flow heat transfer coefficients are instead considerably underpredicted by considering the vapor-only Dittus-Boelter equation. However, it is worth noting that also in this case some of these data, although classified as mist flow according to the Cheng et al. [66] model, may instead belong to a different flow regime, making unsuitable the use of a vapor-only Nusselt number for comparison purposes.

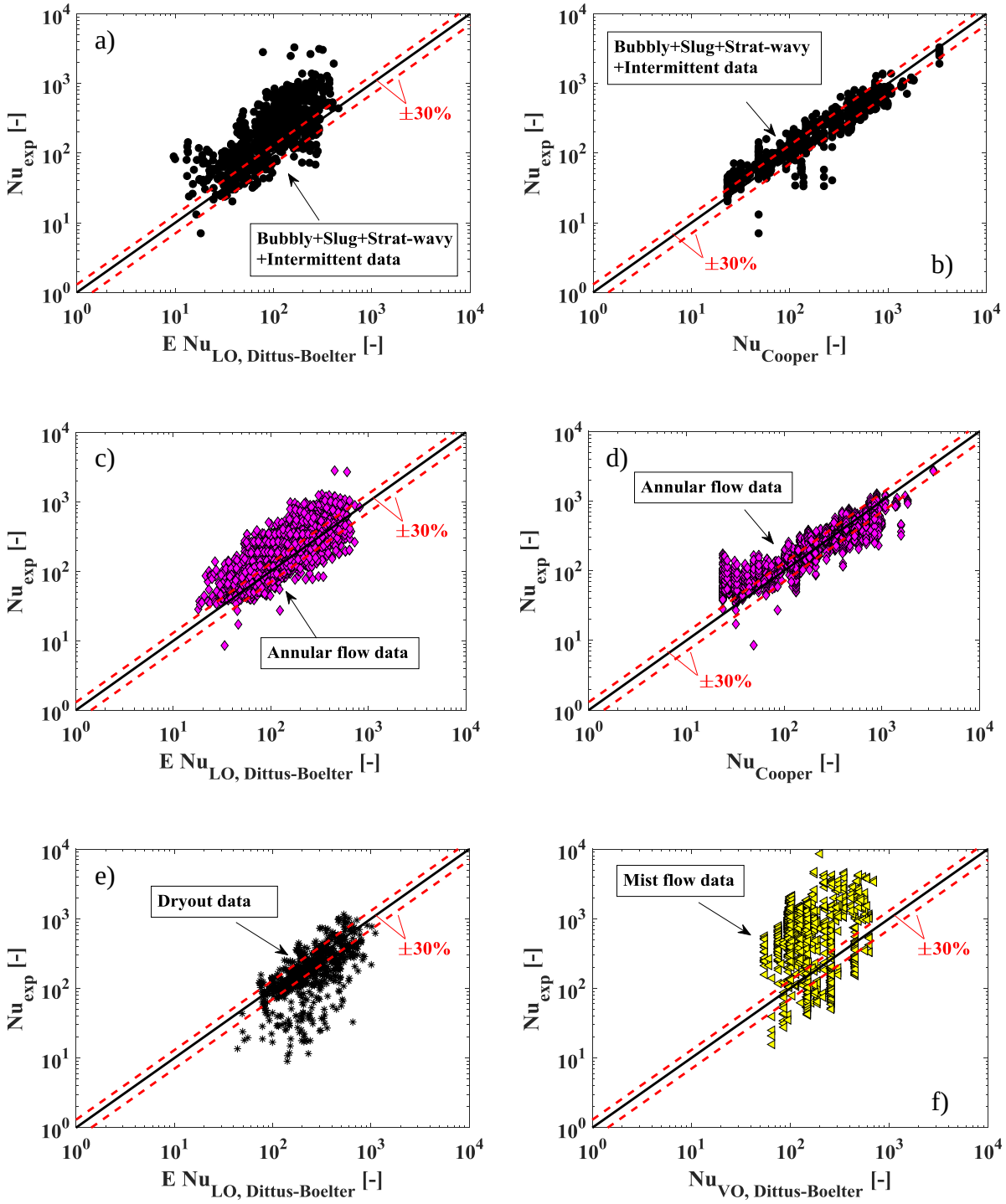

Figure 8 Experimental versus predicted Nusselt numbers, separated by flow pattern. Convective (a) and nucleative (b) boiling contribution for bubbly, slug, stratified-wavy and intermittent flow data. Convective (c) and nucleative (d) boiling contribution for annular flow data. (e) Convective contribution for dryout data. (f) Convective (vapor) contribution for mist flow data

3.2 Assessment of correlations for smooth tubes

Several flow boiling heat transfer prediction methods explicitly developed for carbon dioxide in smooth micro and macro tubes are available in literature. In this review, 12 models are implemented to test their agreement with the experimental data. Unfortunately, missing information in the work of Mikielewicz and Jakubowska [71] made their method not possible to implement for this assessment. The mathematical formulation and range of validity of the chosen correlations are provided in Table 2, whereas their complete assessment is given in Table 3, in which the experimental data are segregated according to their flow pattern and in micro/macro scale. The statistical analysis is carried-out with the calculation of the Mean Absolute Error ($|\eta|$), Mean Relative Error (η), percentage of data points falling into an error range of ±30% (Ψ) and of ±50% (χ). For each bunch of data, the best three working correlations are highlighted in bold and a graphical comparison is also provided in Figure 9a-d.

The previous section has shown that data belonging to bubbly, slug, stratified-wavy and intermittent flow regimes were quite well predicted by only considering the Cooper [67] expression for pure pool boiling Nusselt number (Figure 8b), having a calculated MAE of $|\eta|$=51%. A better agreement is here obtained by implementing the superposition method of Oh et al. [30] (see Figure 9a), that combines the liquid Dittus-Boelter expression to the Cooper heat transfer coefficient. The calculated *MAE* is $|\eta|$=33.3%, with 85% of the points falling in a ±50% error band. Similar good agreements are also found with the correlation of Hihara and Tanaka [72] ($|\eta|$=35.3%) and the superposition model of Choi et al. ($|\eta|$=35.2%). In case of annular flow regime, the best agreement is found with the method of Hihara and Tanaka [72] (see Figure 9b), with calculated $|\eta|$=27%, η=0.9%, ψ=67% and χ=88%, and similar results are obtained with the flow pattern based methods of Thome and El-Hajal [35] and of Cheng et al. [36].

In case of dryout and mist flow, most of the chosen correlations do not work well (ignoring the onset of dryout), and only the flow pattern based prediction methods provide a fair accuracy. The Thome and El-Hajal model [35] best fits the dryout points, with a calculated $|\eta|$=55%, mostly underpredicting the experimental heat transfer coefficients (η=-14.6%), as shown in Figure 9c. The assessment for the mist flow data gives a lowest $|\eta|$ of 73%, obtained with the model developed by Pettersen [42], that uses an asymptotic approach for the pre-dryout points and the Shah and Siddiqui [73] model for the post-dryout heat transfer. The onset of dryout was instead estimated using water data from Kon'kov [74] scaled to CO_2 with the dimensional analysis method of Ahmad [75]. The reason of this very high *MAE* lies in the group of data close to the x-axis in Figure 9d, that are not likely to belong to the mist flow regime, as instead originally sorted using the flow pattern map of Cheng et al. [66], whose dryout-mist flow transition criterion should be therefore modified.

By considering the entire database, the three best working prediction methods are those of Pettersen [42] ($|\eta|$=46%), Cheng et al. [36] ($|\eta|$=52%) and Thome and El-Hajal [35] ($|\eta|$=58%). Their accuracy does not significantly change when used for mini or macrochannels, being consistent to the similar behavior of small and conventional tubes when the effect of the operating parameters was analyzed in the previous section of this review.

Table 2 Mathematical expressions of the flow boiling heat transfer prediction methods for pure carbon dioxide in smooth tubes

Author	Formulation	Range of applicability
Hwang et al. [76]	$h = Sh_{nb} + Eh_{cb}$ Nucleate boiling heat transfer coefficient h_{nb} with Forster-Zuber [77] correlation $h_{cb} = Pr_L^{0.6} \cdot h_L$, liquid heat transfer coefficient h_L with Dittus-Boelter [68] correlation $E = 2 \cdot \left(0.213 + {}^{1}\!/\!_{X_{tt}}\right)^{0.736}$ for $X_{tt} < 10$ $E = 1$ for $X_{tt} \geq 10$ $S = \dfrac{1 - \exp\left(-E \cdot h_L \cdot {}^{X}\!/\!_{\lambda_L}\right)}{E \cdot h_L \cdot {}^{X}\!/\!_{\lambda_L}}$ $X = 0.05 \cdot \sqrt{\dfrac{\sigma}{g\left(\rho_L - \rho_V\right)}}$	$d = 7.0\ mm$ $200 \leq G \leq 400\ kg\ m^{-2}s^{-1}$ $3.0 \leq q \leq 9.0\ kW\ m^{-2}$ $-25 \leq T_{sat} \leq 5\ °C$
Hihara and Tanaka [72]	$h = \left(14700 \cdot Bo + 0.93 \cdot \left({}^{1}\!/\!_{X_{tt}}\right)^{2/3}\right) \cdot h_{LO}$, with h_{LO} evaluated with liquid-only Dittus-Boelter [68] correlation.	$0.7 \leq d \leq 2\ mm$ $360 \leq G \leq 1440\ kg\ m^{-2}s^{-1}$ q and T_{sat} ranges not available
Yoon et al. [26]	$x_{cr} = 38.27 \cdot \left(Re_L\right)^{2.12} \cdot \left(1000Bo\right)^{1.64} \cdot Bd^{-4.7}$ For $x \leq x_{cr}$ $h = \left[\left(Sh_{nb}\right)^2 + \left(Eh_L\right)^2\right]^{1/2}$, with nucleate boiling h_{nb} and liquid h_L heat transfer coefficients evaluated with Cooper [67] and Dittus-Boelter [68], respectively. $E = \left[1 + 9.36 \cdot 10^3 \cdot \mathrm{Pr}_L \left(\dfrac{\rho_L}{\rho_V} - 1\right)\right]^{0.11}$ $S = \left(1 + 1.62 \cdot 10^{-6} \cdot E^{0.69} \cdot \mathrm{Re}_L^{1.11}\right)^{-1}$	$d = 7.73\ mm$ $212 \leq G \leq 530\ kg\ m^{-2}s^{-1}$ $12.3 \leq q \leq 18.9\ kW\ m^{-2}$ $-4 \leq T_{sat} \leq 20\ °C$

	For $x > x_{cr}$ $h = \frac{\theta_{dry} h_V + \left(2\pi - \theta_{dry}\right) E h_L}{2\pi}$, liquid and vapor heat transfer coefficients with Dittus-Boelter [68] equation. $E = 1 + 3000 Bo^{0.86} + 1.12 \left(\frac{x}{1-x}\right)^{0.75} \left(\frac{\rho_L}{\rho_V}\right)^{0.41}$ $\frac{\theta_{dry}}{2\pi} = 36.23 \mathrm{Re}_L^{3.47} Bo^{4.84} Bd^{-0.27} \left(1/X_{tt}\right)^{2.6}$	
Thome and El-Hajal [35]	$h = \frac{\theta_{dry} h_V + \left(2\pi - \theta_{dry}\right) h_{wet}}{2\pi}$, the dry angle θ_{dry} varies from 0 in case of annular flow u to θ_{strat} in case of fully stratified flow. The two angles expressions are available in Kattan et al. [78] [79] $h_V = 0.023 \left(\frac{Gxd}{\alpha \mu_V}\right)^{0.8} \mathrm{Pr}_V^{0.4} \frac{\lambda_V}{d}$, in which the void fraction is obtained with the Rohuani and Axelsson [70] model. $h_{wet} = \left[\left(Sh_{nb,CO_2}\right)^3 + h_{cb}^3\right]^{1/3}$ $h_{nb,CO_2} = 0.71 h_{nb} + 3970$, with nucleate boiling heat transfer coefficient calculated with Cooper [67] equation. $S = \frac{\left(1-x\right)^{0.5}}{0.121 \mathrm{Re}_{LF}^{0.225}}$ $\mathrm{Re}_{LF} = \frac{4G(1-x)\delta}{(1-\alpha)\mu_L}$ $\delta = \frac{d}{4}(1-\alpha)$ $h_{cb} = 0.0133 \cdot \mathrm{Re}_{LF}^{0.69} \mathrm{Pr}_L^{0.4} \frac{\lambda_L}{\delta}$	$0.79 \le d \le 10.06\ mm$ $85 \le G \le 1440\ kg\ m^{-2} s^{-1}$ $5 \le q \le 36\ kW\ m^{-2}$ $-25 \le T_{sat} \le 25\ °C$

Pettersen [42]	For $x \le x_{cr}$: $h = \left(h_{nb}^3 + h_{cb}^3\right)^{1/3}$, with nucleate boiling heat transfer coefficient h_{nb} evaluated with Cooper [67] equation and the convective boiling heat transfer coefficient estimated with Kattan et al. [78] [79] flow pattern based model. Post-dryout region ($x \ge x_{cr}$) heat transfer coefficient calculated with Shah and Siddiqui [73] model. Dryout vapor quality x_{cr} using Kon'kov [74] expression for H_20 and Ahmad [75] fluid-to-fluid scaling model	$d = 0.8\ mm$ $190 \le G \le 570\ kg\ m^{-2}s^{-1}$ $5 \le q \le 20\ kW\ m^{-2}$ $0 \le T_{sat} \le 25\ °C$
Choi et al. [28]	$h = Sh_{nb} + Eh_L$, with nucleate boiling h_{nb} and liquid h_L heat transfer coefficients evaluated with Cooper [67] and Dittus-Boelter [68], respectively. $S = 7.2694\left(\phi^2\right)^{0.0094} Bo^{0.2814}$ $E = 0.05 \cdot \left(\phi^2\right) + 0.95$ $\phi^2 = 1 + \frac{C}{X_{tt,Choi}} + \frac{1}{X_{tt,Choi}^2}$, with the Chisholm parameter *C* set to 20, 12, 10 and 5 in case of liquid-vapor flow condition of turbulent-turbulent, laminar-turbulent, turbulent-laminar and laminar-laminar, respectively $X_{tt,Choi} = \left(\frac{1-x}{x}\right)^{7/8}\left(\frac{\rho_V}{\rho_L}\right)^{0.5}\left(\frac{\mu_L}{\mu_V}\right)^{1/8}$.	$1.5 \le d \le 3.0\ mm$ $400 \le G \le 500\ kg\ m^{-2}s^{-1}$ $30 \le q \le 40\ kW\ m^{-2}$ $-10 \le T_{sat} \le -5\ °C$
Choi et al. II [29]	Same expression as Choi et al. [28], with a different evaluation of the suppression and enhancement factors: $S = 469.1689\left(\phi^2\right)^{-0.2093} Bo^{0.7402}$ $E = 0.042 \cdot \left(\phi^2\right) + 0.958$	$1.5 \le d \le 3.0\ mm$ $200 \le G \le 600\ kg\ m^{-2}s^{-1}$ $10 \le q \le 40\ kW\ m^{-2}$ $T_{sat} = 10\ °C$ $fluids: CO_2, R134a, R22$
Cheng et al. [66] [36]	For any flow pattern except dryout and mist flow: $h = \frac{\theta_{dry} h_V + \left(2\pi - \theta_{dry}\right) h_{wet}}{2\pi}$, vapor heat transfer coefficient h_V with Dittus-Boelter [68] equation. $\theta_{dry} = 0$ for bubbly, slug intermittent and annular flow regimes; $\theta_{dry} = \theta_{strat}\left(\frac{G_{wavy} - G}{G_{wavy} - G_{strat}}\right)^{0.61}$ for stratified-wavy flow;	$0.6 \le d \le 10.06\ mm$ $80 \le G \le 1500\ kg\ m^{-2}s^{-1}$ $4 \le q \le 46\ kW\ m^{-2}$ $-28 \le T_{sat} \le 25\ °C$

$$\theta_{dry} = \theta_{strat} \frac{x}{x_{IA}} \left(\frac{G_{wavy} - G}{G_{wavy} - G_{strat}} \right)^{0.61}$$ for slug/stratified-wavy flow, in case $x < x_{IA}$

Flow patterns, stratified angle θ_{strat}, intermittent to annular quality transition x_{IA}, stratified to stratified-wavy flow transition G_{strat} and the stratified-wavy to intermittent and annular flow transition G_{wavy} are obtainable in the original reference.

$h_{wet} = \left[\left(Sh_{nb} \right)^3 + h_{cb}^3 \right]^{1/3}$, with convective boiling heat transfer coefficient h_{cb} as in Thome and El-Hajal [35].

$$h_{nb} = 131 P_{red}^{-0.0063} \left(-\log_{10} \left(P_{red} \right) \right)^{-0.55} M^{-0.5} q^{0.58}$$

$S = 1$ for $x < x_{IA}$

$$S = 1 - 1.14 \left(\frac{d}{0.00753} \right)^2 \left(1 - \frac{\delta}{\delta_{IA}} \right)^{2.2}$$ for $x \geq x_{IA}$, with δ_{IA} using the following δ expression at the intermittent to annular flow transition.

$$\delta = \frac{d}{2} - \sqrt{\left(\frac{d}{2} \right)^2 - \frac{\pi d^2 (1-\alpha)}{2(2\pi - \theta_{dry})}}$$.

In case of mist flow regime:

$$h_{mist} = 2 \cdot 10^{-8} \, \mathrm{Re}_H^{1.97} \, \mathrm{Pr}_V^{1.06} \, Y^{-1.83} \frac{\lambda_V}{d}$$

$$\mathrm{Re}_H = \frac{Gd}{\mu_V} \left[x + \frac{\rho_V}{\rho_L} (1 - x) \right]$$

$$Y = 1 - 0.1 \left[\left(\frac{\rho_V}{\rho_L} - 1 \right) (1 - x) \right]^{0.4}$$

In case of dryout flow regime:

$$h_{dryout} = h(x_{di}) - \frac{x - x_{di}}{x_{de} - x_{di}} \left[h(x_{di}) - h_{mist}(x_{de}) \right]$$

$$x_{di} = 0.58 \exp \left[0.52 - 0.236 \left(\frac{G^2 d}{\rho_V \sigma} \right)^{0.17} \left(\frac{G^2}{g \rho_V (\rho_L - \rho_V) d} \right)^{0.17} \left(\frac{\rho_V}{\rho_L} \right)^{0.25} \left(\frac{q}{q_{cr}} \right)^{0.27} \right]$$

	$x_{de} = 0.61\exp\left[0.57 - 0.502\left(\frac{G^2 d}{\rho_V \sigma}\right)^{0.16}\left(\frac{G^2}{g\rho_V(\rho_L-\rho_V)d}\right)^{0.15}\left(\frac{\rho_V}{\rho_L}\right)^{-0.09}\left(\frac{q}{q_{cr}}\right)^{0.72}\right]$ $q_{cr} = 0.131\rho_V^{0.5} i_{LV}\left[g\sigma(\rho_L-\rho_V)\right]^{0.25}$	
Yun and Kim [25]	$h = 16.26 \cdot q^{0.72} \cdot P_{red}^{0.88}$, for $\delta \geq \delta_{cr}$ $h = 1.09 \cdot 10^{-3}\frac{\lambda_V}{d}\left[\mathrm{Re}_{VO}\left(x + \frac{\rho_V}{\rho_L}(1-x)\right)\right]^{0.989} \mathrm{Pr}_V^{1.41} Y^{-1.15}$, for $\delta < \delta_{cr}$ $Y = 1 - 0.1\left[\left(\frac{\rho_V}{\rho_L} - 1\right)(1-x)\right]^{0.4}$ $\delta = \frac{d}{2}\left(1-\alpha^{0.5}\right)$ $\delta_{cr} = \left(\frac{3}{4}\left(\frac{\mu_L}{\rho_L}\right)^2 \frac{1}{g}\mathrm{Re}_L\right)^{1/3}$	$0.98 \leq d \leq 2.0\ mm$ $360 \leq G \leq 1500\ kg\ m^{-2}s^{-1}$ $18 \leq q \leq 40\ kW\ m^{-2}$ $0 \leq T_{sat} \leq 15\ °C$
Oh et al. [30]	$h = Sh_{nb} + Eh_L$, with nucleate boiling heat transfer coefficient h_{nb} evaluated with Cooper [67] expression. $S = 0.279\left(\phi^2\right)^{-0.029} Bo^{-0.098}$ $E = \max\left[\left(0.023\phi^{2.2} + 0.76\right), 1\right]$ $\phi^2 = 1 + \frac{C}{X} + \frac{1}{X^2}$, with the Chisholm parameter *C* set to 20, 12, 10 and 5 in case of liquid-vapor flow condition of turbulent-turbulent, laminar-turbulent, turbulent-laminar and laminar-laminar, respectively. $X = \left(\frac{f_L}{f_V}\right)^{0.5}\left(\frac{1-x}{x}\right)\left(\frac{\rho_V}{\rho_L}\right)^{0.5}$, with $f = 16/\mathrm{Re}$ for laminar flows and $f = 0.049\,\mathrm{Re}^{-0.25}$ for turbulent flows. $h_L = 4.36\frac{\lambda_L}{d}$ for $\mathrm{Re}_L < 230$	$0.5 \leq d \leq 3.0\ mm$ $200 \leq G \leq 600\ kg\ m^{-2}s^{-1}$ $5 \leq q \leq 40\ kW\ m^{-2}$ $0 \leq T_{sat} \leq 20\ °C$ $fluids: CO_2, R134a,$ $R22, R410A, R290$

	$h_L = \dfrac{(\mathrm{Re}_L - 1000)\,\mathrm{Pr}_L \left(\dfrac{f_L}{2}\right)\left(\dfrac{\lambda_L}{d}\right)}{1+12.7\left(\mathrm{Pr}_L^{2/3}-1\right)\left(\dfrac{f_L}{2}\right)^{0.5}}$ for $3000 \le \mathrm{Re}_L \le 10^4$ $h_L = \dfrac{\mathrm{Re}_L\,\mathrm{Pr}_L \left(\dfrac{f_L}{2}\right)\left(\dfrac{\lambda_L}{d}\right)}{1+12.7\left(\mathrm{Pr}_L^{2/3}-1\right)\left(\dfrac{f_L}{2}\right)^{0.5}}$ for $10^4 \le \mathrm{Re}_L \le 5\cdot 10^6$ $h_L = 0.023\,\mathrm{Re}_L^{0.8}\,\mathrm{Pr}_L^{0.4}\left(\dfrac{\lambda_L}{d}\right)$ for $\mathrm{Re}_L \ge 5\cdot 10^6$	
Pamitran et al. [80]	Same model as Oh et al. [30], with a different evaluation of the enhancement and suppression factors: $S = 0.25\left(\phi^2\right)^{-0.2093} Bo^{0.7402}$ $E = \max\left[\left(0.009\phi^{2.2} + 0.76\right), 1\right]$	$1.5 \le d \le 3.0\ mm$ $50 \le G \le 600\ kg\ m^{-2}s^{-1}$ $5 \le q \le 70\ kW\ m^{-2}$ $0 \le T_{sat} \le 10\ °C$
Ducoulombier et al. [47]	$h = \max\left(\left[h_{nb}, h_{cb}\right]\right)$, with nucleate boiling heat transfer coefficient evaluated with the model of Cheng et al. [66] [36]; $h_{cb} = h_{LO}\left(1.47\cdot 10^4\, Bo + 0.93\left(1/X_{tt}\right)^{2/3}\right)$, for $Bo > 1.1\cdot 10^{-4}$ $h_{cb} = h_L\left(1+1.80\left(1/X_{tt}\right)^{0.986}\right)$, for $Bo < 1.1\cdot 10^{-4}$ The liquid h_L and liquid-only h_{LO} heat transfer coefficients evaluated with Dittus-Boelter [68] equation.	$d = 0.529\ mm$ $200 \le G \le 1200\ kg\ m^{-2}s^{-1}$ $10 \le q \le 30\ kW\ m^{-2}$ $-10 \le T_{sat} \le 0\ °C$

Table 3 Assessment of the CO_2 flow boiling heat transfer coefficient prediction methods for smooth tubes (along the columns), compared to the experimental database separated by the operative conditions (along the rows)

Author	**Hwang et al.** [76]	**Hihara and Tanaka** [72]	**Yoon et al.** [26]	**Thome and El-Hajal** [35]	**Pettersen** [42]	**Choi et al.** [28]	**Choi et al. II** [29]	**Cheng et al.** [66] [36]	**Yun and Kim** [25]	**Oh et al.** [30]	**Pamitran et al.** [80]	**Ducoulombier et al.** [47]
Bubbly, stratified-wavy, slug, intermittent flow regimes	|η|=162 η=160 ψ=14.8 χ=27.4	**|η|=35.3** **η=-11.5** **ψ=51.5** **χ=81.9**	|η|=49.0 η=23.8 ψ=51.4 χ=70.9	|η|=59.2 η=50.4 ψ=45.6 χ=65.7	|η|=36.5 η=20.5 ψ=63.3 χ=80.2	**|η|=35.2** **η=16.9** **ψ=62.1** **χ=79.2**	|η|=36.9 η=2.03 ψ=52.5 χ=83.2	|η|=56.2 η=43.8 ψ=56.5 χ=73.8	|η|=45.9 η=-14.5 ψ=44.3 χ=66.0	**|η|=33.3** **η=-2.26** **ψ=57.1** **χ=85.2**	|η|=71.1 η=-70.6 ψ=5.88 χ=12.1	|η|=38.5 η=26.9 ψ=60.6 χ=77.2
Annular flow regime	|η|=116 η=113 ψ=28.9 χ=42.2	**|η|=27.0** **η=0.92** **ψ=67.0** **χ=87.9**	|η|=31.6 η=4.86 ψ=58.5 χ=83.6	**|η|=27.7** **η=-12.8** **ψ=60.1** **χ=89.5**	|η|=33.2 η=4.00 ψ=59.2 χ=83.3	|η|=33.2 η=15.2 ψ=61.8 χ=80.1	|η|=31.7 η=-15.1 ψ=49.6 χ=86.4	**|η|=31.6** **η=5.84** **ψ=60.8** **χ=85.6**	|η|=73.0 η=-53.9 ψ=20.0 χ=27.0	|η|=35.2 η=-15.9 ψ=43.0 χ=73.1	|η|=78.7 η=-78.7 ψ=0.19 χ=2.26	|η|=32.2 η=19.2 ψ=65.3 χ=81.5
Dryout flow regime	|η|=157 η=151 ψ=38.9 χ=44.9	|η|=92.4 η=86.2 ψ=48.6 χ=58.5	|η|=67.3 η=12.2 ψ=30.2 χ=57.9	**|η|=55.2** **η=-14.6** **ψ=23.6** **χ=62.6**	**|η|=61.8** **η=-25.2** **ψ=18.7** **χ=47.5**	|η|=88.2 η=72.2 ψ=41.8 χ=58.5	|η|=63.3 η=22.8 ψ=34.2 χ=72.7	**|η|=61.3** **η=-30.1** **ψ=21.3** **χ=39.9**	|η|=85.6 η=-81.1 ψ=3.88 χ=5.88	|η|=71.2 η=20.4 ψ=26.5 χ=51.9	|η|=74.1 η=-66.5 ψ=3.88 χ=10.9	|η|=84.9 η=78.2 ψ=51.3 χ=59.2
Mist flow regime	|η|=255 η=251 ψ=28.5 χ=34.7	|η|=251 η=249 ψ=20.2 χ=28.6	|η|=171 η=124 ψ=18.4 χ=33.7	|η|=135 η=87.7 ψ=18.0 χ=41.6	**|η|=72.7** **η=-1.87** **ψ=17.1** **χ=40.9**	|η|=233 η=226 ψ=27.9 χ=35.9	|η|=200 η=178 ψ=21.9 χ=42.8	**|η|=90.7** **η=-46.4** **ψ=7.91** **χ=12.6**	**|η|=78.9** **η=-50.7** **ψ=8.74** **χ=17.0**	|η|=201 η=168 ψ=16.8 χ=34.4	|η|=96.6 η=-0.99 ψ=9.05 χ=17.3	|η|=238 η=235 ψ=24.6 χ=31.9
Macro-channels (Co<0.5)	|η|=212 η=210 ψ=12.0 χ=19.5	|η|=82.6 η=58.1 ψ=43.6 χ=65.7	|η|=67.9 η=40.9 ψ=46.8 χ=69.9	**|η|=55.6** **η=19.2** **ψ=47.2** **χ=74.2**	**|η|=47.5** **η=8.69** **ψ=41.7** **χ=61.6**	|η|=86.6 η=75.8 ψ=40.6 χ=57.8	|η|=65.0 η=36.2 ψ=48.9 χ=73.7	**|η|=52.4** **η=21.5** **ψ=44.4** **χ=66.0**	|η|=57.6 η=-26.5 ψ=31.3 χ=44.4	|η|=65.1 η=38.5 ψ=50.9 χ=72.9	|η|=80.4 η=-61.9 ψ=2.71 χ=7.80	|η|=88.3 η=80.4 ψ=40.2 χ=58.2
Micro-channels (Co>0.5)	|η|=87.7 η=82.2 ψ=48.3 χ=62.7	|η|=76.9 η=58.3 ψ=64.4 χ=78.3	|η|=63.0 η=18.1 ψ=43.3 χ=66.0	**|η|=60.9** **η=13.5** **ψ=39.6** **χ=69.5**	**|η|=43.4** **η=-8.82** **ψ=53.3** **χ=78.7**	|η|=70.0 η=47.8 ψ=67.2 χ=81.6	|η|=73.0 η=20.7 ψ=34.4 χ=77.9	**|η|=50.5** **η=-33.0** **ψ=43.4** **χ=58.8**	|η|=89.1 η=-82.1 ψ=4.51 χ=8.12	|η|=78.7 η=10.1 ψ=21.5 χ=54.3	|η|=79.6 η=-60.3 ψ=4.12 χ=8.25	|η|=68.6 η=56.5 ψ=72.7 χ=80.2
Overall database	|η|=157 η=153 ψ=28.1 χ=38.7	|η|=80.0 η=58.2 ψ=52.9 χ=71.3	|η|=65.7 η=30.8 ψ=45.3 χ=68.2	**|η|=58.0** **η=16.7** **ψ=43.8** **χ=72.1**	**|η|=45.7** **η=0.91** **ψ=45.5** **χ=69.2**	|η|=79.1 η=63.4 ψ=52.4 χ=68.4	|η|=68.6 η=29.3 ψ=42.5 χ=75.6	**|η|=51.6** **η=-2.87** **ψ=44.0** **χ=62.8**	|η|=71.6 η=-51.2 ψ=19.4 χ=28.3	|η|=71.1 η=25.9 ψ=37.8 χ=64.6	|η|=80.0 η=-61.2 ψ=3.34 χ=8.00	|η|=79.5 η=69.7 ψ=54.6 χ=68.0

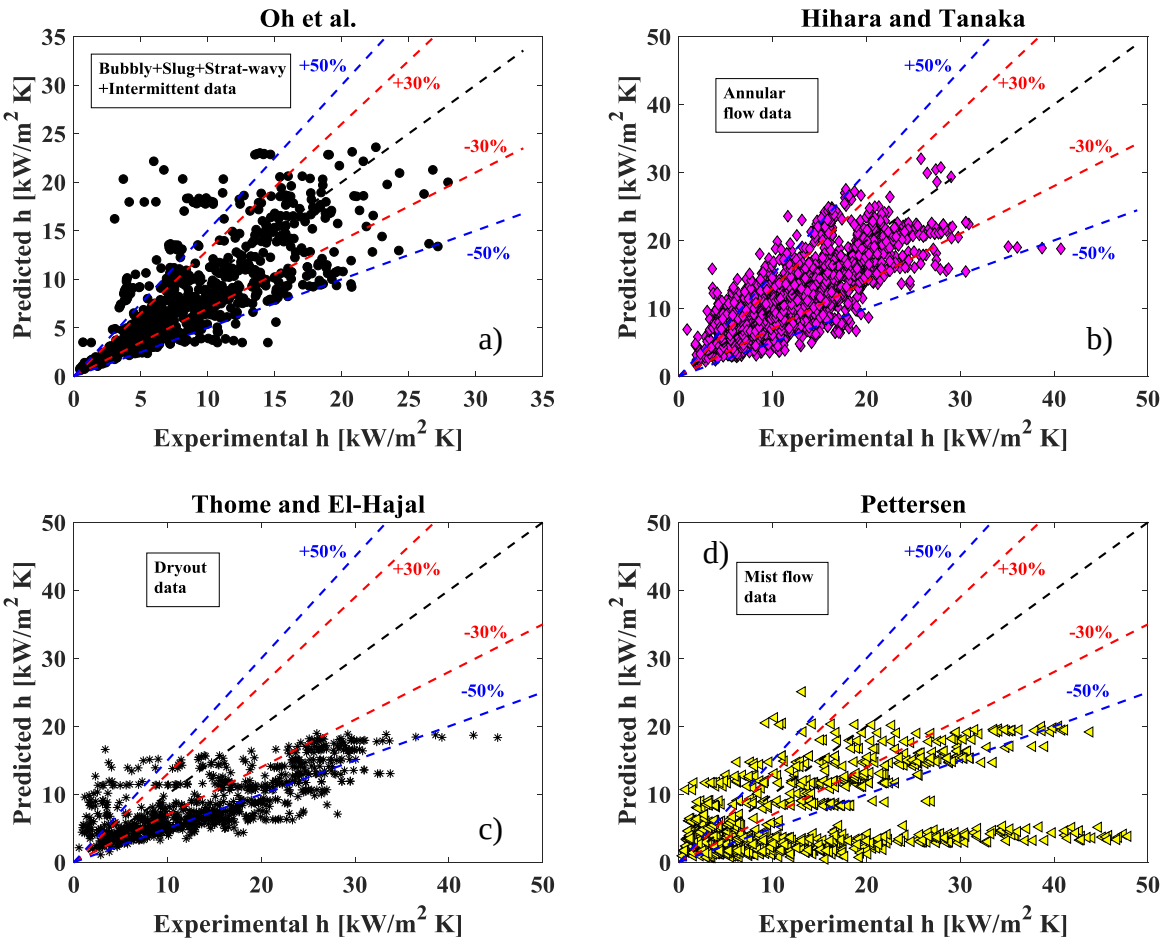

Figure 9 Experimental versus predicted heat transfer coefficients for smooth tubes according to the best working correlations, separated by flow pattern.

4. Boiling of CO_2 in enhanced surfaces and with the presence of oil

4.1 Experimental database for microfin tubes

The research has highlighted 10 flow boiling studies in microfinned surfaces using pure carbon dioxide as working fluid, from 2005 until 2015, by collecting a total amount of 883 heat transfer coefficient data. The whole database is shown in Table 4: tests have been performed with different kinds of geometrical characteristics, covering mass fluxes from 75 to 800 kg/m^{2}s, saturation temperatures from -30 to +20 °C, heat fluxes from 1.67 to 61 kW/m^2, with and single/multi tube diameters from 0.8 mm to 11.2 mm. All the experiments have been conducted in circular and horizontal channels.

Schael and Kind [52] performed CO_2 flow boiling experiments with a microfin 8.62 mm tube made up of 60 fins with a 18° helix angle. The authors observed that convection was promoted by the helical grooves, with increasing heat transfer coefficients with mass flux. On the other hand, the bubble formation was seen to be suppressed.

Microfin tubes with similar geometrical characteristics were investigated by Cho et al. [53] [54], together with smooth pipes having the same internal diameters. The heat transfer coefficients in the microfin channels were found 150-210% higher than those in the smooth tubes at the same test conditions. The authors attributed this behavior to a larger heated surface and a promoted annular flow regime by means of the fin structure.

Gao et al. [56] performed a comprehensive investigation on flow boiling of carbon dioxide in smooth and enhanced tubes of 3 mm ID, with and without the presence of oil. In case of pure CO_2, the heat transfer coefficients showed a strong dependency on heat flux and a negligible influence of the mass velocity for both smooth and microfin tube. Indeed, dryout vapor quality was seen to decrease with mass flux in the smooth channel, whereas no changes were observed in the enhanced tube.

A peculiar grooved multi-port test section was tested by Jeong and Park [43], made up of 8 minichannels with an internal diameter of 0.8 mm, together with a similar structure having 6 smooth narrow circular tubes for comparison purposes. Some details of this test section are shown in Figure 10a. It was found that at lower vapor qualities (x<0.3), the heat transfer was considerably enhanced by the micro-grooves (+320%), especially in case of high saturation temperatures. At higher qualities, however, the grooves showed a negative effect on the heat transfer coefficient. A multi-microfin tube test section with zero helix angle was also used by Wu et al. [44] in their investigation on flow boiling heat transfer and pressure drop with pure CO_2. The authors reported a significant influence of the heat flux and of the saturation temperature, which increased the heat transfer coefficient but also tended to anticipate the onset of dryout.

Dang et al. [81] studied the effect of the operating parameters in a with a 2 mm microfin tube, whose picture is shown in Figure 10b. The heat transfer coefficients were also compared to the values obtained in a smooth tube at the same operating conditions, as presented in Figure 11a. It was found that the use of fins was able to enhance the turbulence of the liquid phase, conveyed further in the tube and thus delaying the dryout occurrence with respect to the smooth tube.

A similar behavior was found by Zhao and Bansal [82], that performed flow boiling experiments in a 7.31 mm microfin tube at a single low saturation temperature of -30 °C, thus working with a reduced pressure similar to that of halogenated refrigerants at higher temperatures.

Finally, Kim et al. [83], in their 11.2 mm microfin tube, found that the carbon dioxide heat transfer coefficient trend with vapor quality was altered by the presence of fins, as shown in Figure 11b. The authors stated that the internal tube peculiar structure was able to drive the liquid phase in the grooves, thus anticipating the appearance of the annular flow regime and providing a convective behavior. This was also corroborated by the flow patterns observations carried out in their work.

a) b)

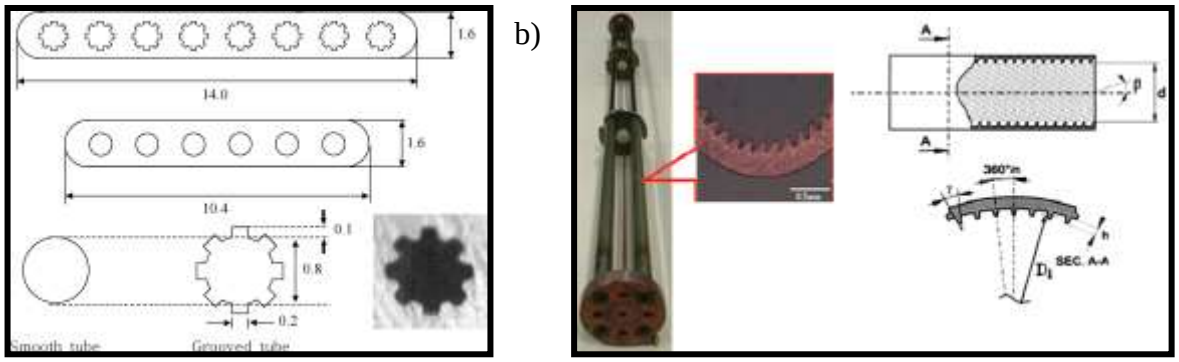

Figure 10 Examples of enhanced surfaces for flow boiling of CO_2. (a) Grooved multi-port test section of Jeong and Park **[43]** and reference smooth multi-port mini-tubes. Measurements are in mm. (b) Single microfin tube of Dang et al. **[81]**

Table 4 Experimental databank for boiling of CO_2 in enhanced tubes

Author	**Geometry***	**Internal diameter [mm]**	**Mass velocity [kg m^{-2} s^{-1}]**	**Heat flux [kWm^{-2}]**	**Saturation temperature [°C]**	**Number of points**
Schael and Kind [52]	S,C,H microfinned: Fin height=0.25mm Helix angle=18° Fins=60 Fin tip angle=30°	8.62	75/500	3.9/61	5	30
Cho et al. [53] [54]	S,C,H microfinned: Fin height=0.15mm Helix angle=18° Fins=60	4.4/8.92	212/656	6/30	-5/20	200
Gao et al. [56]	S,C,H microfinned: Fin height=0.11mm Helix angle=12° Fins=40 Fin tip angle=40.5°	3.04	190/770	10/30	10	71
Jeong and Park [43]	M,C,H grooved: depth=0.1mm width=0.2	0.8	400/800	12/18	0/10	51
Dang et al. [81]	S,C,H microfinned: Fin height=0.12mm Helix angle=6.3° Fins=40 Fin tip angle=34.8°	2	360/720	4.5/18	15	185
Ono et al. [61]	S,C,H microfinned: Fin height=0.11mm Helix angle=12° Fins=50 Fin tip angle=40°	3.75	190/380	10/30	10	58
Zhao and Bansal [82]	S,C,H microfinned: Fin height=0.20mm Helix angle=18° Fins=50 Fin tip angle=52°	7.31	100/250	9.9/30	-30	82
Kim et al. [83]	S,C,H microfinned: Helix angle=30° Fins=68	11.2	100/200	10	-15	11
Wu et al. [44]	M,C,H microfinned: Fin height=0.16mm Helix angle=0° Fins=13 Fin tip angle=30	1.7	100/600	1.67/8.33	1/15	195
Overall		**0.8/11.2**	**75/800**	**1.67/61**	**-30/20**	**883**
**M=multi, S=single; C=circular, R=rectangular; H=horizontal, V=vertical*						

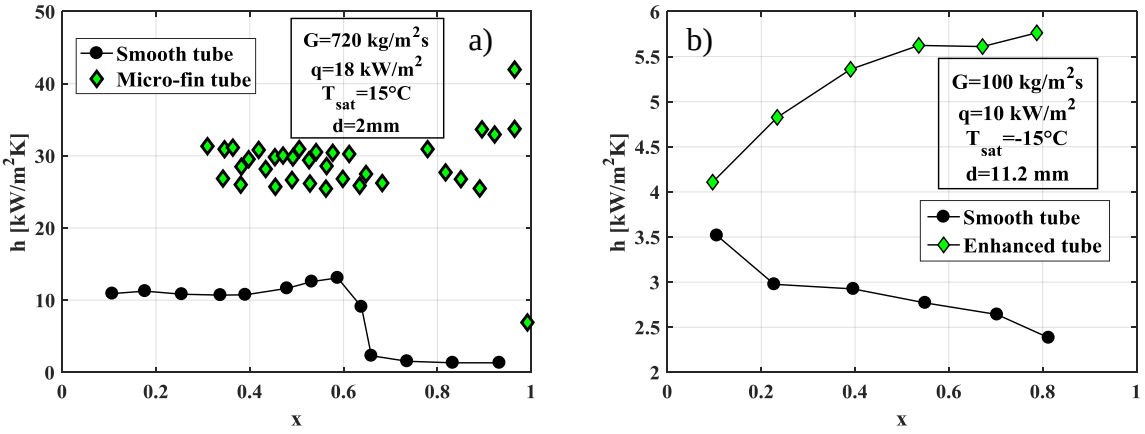

Figure 11 Effect of the microfin structure on flow boiling heat transfer of CO_2. (a) Heat transfer enhancement and delayed dryout. Data from Dang et al. **[81]**. (b) Improved convection. Data from Kim et al. **[83]**

4.2 Heat transfer for CO_2/oil mixtures in smooth tubes

The presence of oil in refrigeration systems is often required for a correct lubrication of the operating devices. The choice of a suitable oil is always a demanding issue, and in case of carbon dioxide it is complicated by its higher reduced pressure and peculiar physical properties. In terms of miscibility, the following lubricants are expected [6] to provide the highest solubility, in decreasing order: POE, ester oils, PVE, PAG, AB, POA and mineral oil (CO_2 is immiscible with mineral lubricants). Nevertheless, most of the reports available do not cover wide ranges of temperature and/or concentration and the phase equilibrium and thermodynamic properties behavior are strictly associated to the operating conditions and the type of oil employed. Seeton et al. [84] found that PAG, AB and PAO lubricants were not miscible with CO_2 at high refrigerant concentrations, whereas POE oil provided complete miscibility in the range -20/+120 °C. Hauk and Weidner [85], instead, observed the coexistence of two liquid phases for three different oils (POE, PAG and PAO) over a range of 5/100 °C. Whichever lubricant chosen, during the normal operation of a refrigeration system a non-negligible amount of oil may drift from the compressor moving parts to the heat exchangers, altering the heat transfer behavior of the working fluid because of the modification of the thermodynamic and transport properties for the mixture.

Wang et al. [86] published a comprehensive review to summarize the general trends of the lubricant presence on the evaporating heat transfer coefficient of halogenated refrigerants and CO_2. They concluded that the influence of oil depends not only on its concentration, but also on the heat flux, mass flux and other operating parameters. As a fact, it is difficult to provide general indications due to the large difference of properties in the available commercial lubricants, and different studies may therefore provide inconsistencies.

Table 5 summarizes the flow boiling heat transfer coefficient data for CO_2/oil mixtures in smooth tubes collected for this review. PAG and POE type lubricants have been used for nominal mass concentrations ω_0 from 0.1% to 5% in tubes of diameters from 2 to 11.2 mm in different operating conditions in terms of mass flux (from 100 to 1400 kg/m^{2}s), saturation temperature (from -30 to 15 °C) and heat flux (from 0.5 to 36 kW/m^2), for a total amount of 1184 data points. All the experiments refer to single, circular and horizontal tubes.

In the study of Gao et al. [56], performed with PAG oil in a 3.0 mm tube, the CO_2 local heat transfer coefficients were seen to decrease with vapor quality and they were considerably lower for oil concentrations higher than 0.11%. The authors also found PAG oil to be immiscible or only partially miscible with carbon dioxide for their operating conditions.

Pehlivanoglu et al. [59] pointed out that the presence of lubricant strongly reduced the nucleative boiling contribution, as shown in their experimental data in Figure 12a at moderate heat and mass fluxes, in which the heat transfer coefficient passes from approximately 9 kW/m^{2}K up to 7.5 kW/m^{2}K (-18%) when a small nominal oil mass fraction of 2% is considered. This behavior can be explained with the simultaneous significant increase of the saturation temperature and of the liquid surface tension for the refrigerant/oil mixture, both penalizing the bubble nucleation with a higher superheat required with respect to the pure fluid at the same operating conditions. Similar trends and strong penalizations of the nucleate boiling heat transfer coefficient with increasing oil concentration are also found in most of the data collected [57] [61] [62]. It is important to remark that the increase of the saturation temperature for the oil/CO_2 mixture leads to an intrinsic error in the data reduction procedure. For all the experimental studies reviewed, in fact, the flow boiling heat transfer coefficient is obtained according to Equation (8), thus incorrectly using the saturation temperature of the pure carbon dioxide.

$$h = \frac{q}{T_{wall} - T_{sat}} \tag{8}$$

As suggested by Thome et al. [87] [88], one should use instead the mixture saturation temperature $T_{sat,m}$ as shown in Equation (9), which could significantly increase with proceeding evaporation, as a function of the local oil mass concentration, defined in Equation (10).

$$h = \frac{q}{T_{wall} - T_{sat,m}} \tag{9}$$

$$\omega_{oil,x} = \frac{\omega_0}{1-x} \tag{10}$$

However, as experimented by [89] and [90], the saturation temperature remains almost unchanged with both POE and PAG lubricants up to local oil mass concentrations of 50-70%, that are reached, for the present database ($\omega_0 \leq 5\%$), only at very high vapor qualities ($x > 0.90$).

In some cases, a positive effect of the presence of oil for high vapor qualities has been observed, as shown in Figure 12c for the data of Kim et al. [60] with POE lubricant in a 11.2 mm tube. In case of pure CO_2, the low mass flux of 100 kg/m^{2}s leads to a decreasing heat transfer coefficient trend with vapor quality for pure CO_2, due to the growth of the dryout region on the top of the tube in a stratified flow. When oil is added, the higher liquid surface tension of the mixture tends to increase the wetted fraction of the tube wall, thus shaping an annular flow and a convective heat transfer behavior.

Table 5 Experimental databank for boiling of CO_2 in smooth tubes with the presence of oil

Author	**Geometry***	**Internal diameter [mm]**	**Mass velocity [kg m^{-2} s^{-1}]**	**Heat flux [kW m^{-2}]**	**Saturation temperature [°C]**	**Oil mass fraction [%]**	**Oil type**	**Number of points**
Gao et al. [56]	S,C,H	3	193/1094	10/20	10	0.11/0.57	PAG	45
Katsuta et al. [57]	S,C,H	3	400	5/15	0/10	0.3/3.5	PAG VG100	164
Pehlivanoglu et al. [59]	S,C,H	6.1	100/400	2/15	-30/-15	0.5/2	POE C85	179
Kim et al. [60] [83]	S,C,H	11.2	100/200	0.5/10	-15	0.5/2	POE RENSIO C85	117
Ono et al. [61]	S,C,H	3.76	100/380	10/30	10/10	0.1/1	PAG	151
Dang et al. [62]	S,C,H	2/6	360/1440	4.5/36	15	0.5/5	PAG 100	528
Overall		**2/11.2**	**100/1440**	**0.5/36**	**-30/15**	**0.1/5**		**1184**
**M=multi, S=single; C=circular, R=rectangular; H=horizontal, V=vertical*								

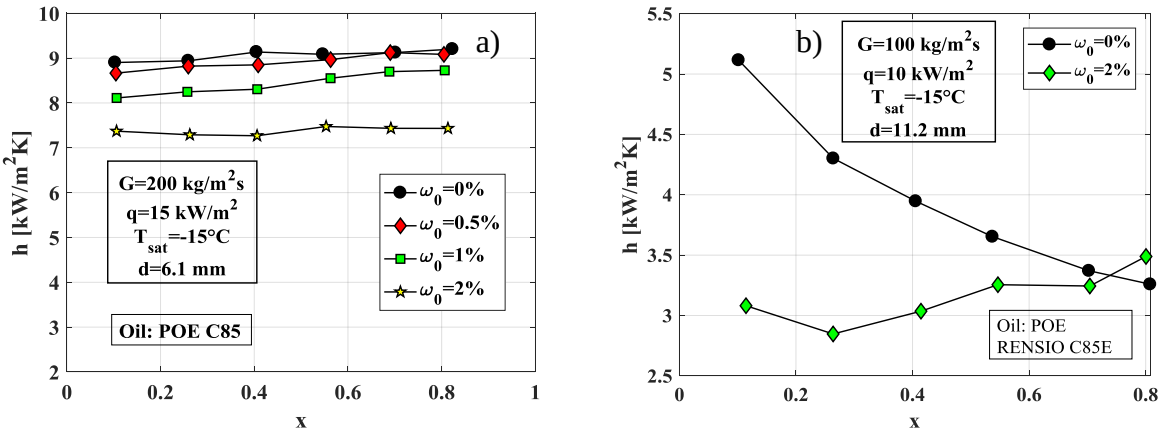

Figure 12 Effect of lubricating oil on flow boiling heat transfer of CO_2. (a) Reduction of the nucleative boiling contribution. Data from Pehlivanoglu et al. **[59]**. (b) Slight enhancement of convection. Data from Kim et al. **[60]**

5. Assessment of prediction methods for enhanced surfaces and oil effect

5.1 Nucleate and convective boiling contributions

Figure 13a-e presents a bar chart distribution for both databases including microfin tubes and smooth tubes with the presence of oil. 883 data points in enhanced surfaces and 1184 heat transfer coefficient values for CO_2/oil mixtures are segregated into different categories according to their operating conditions, in terms of tube internal diameter, mass flux, saturation temperature, heat flux and nominal oil mass fraction ω_0. For the microfin tube database, a consistent amount of experimental points are collected with diameters of 1.7 and 2.0 mm (43% of the entire databank) and for the saturation temperatures of 15 °C (35% of the databank), all belonging to the studies of Wu et al. [44] and of Dang et al. [81]. As for the CO_2/oil heat transfer coefficient data, remarkable peaks are found for saturation temperatures of -15 °C, 10 °C and 15 °C and for imposed heat fluxes of 10, 18 and 36 kW/m^2, due to the comprehensive experimental investigation of Dang et al. [62] that represents alone the 45% of the entire CO_2/oil collected database. Finally, more than 550 points are taken at a nominal oil mass fraction of 1.0%, including both synthetic PAG and POE lubricants.

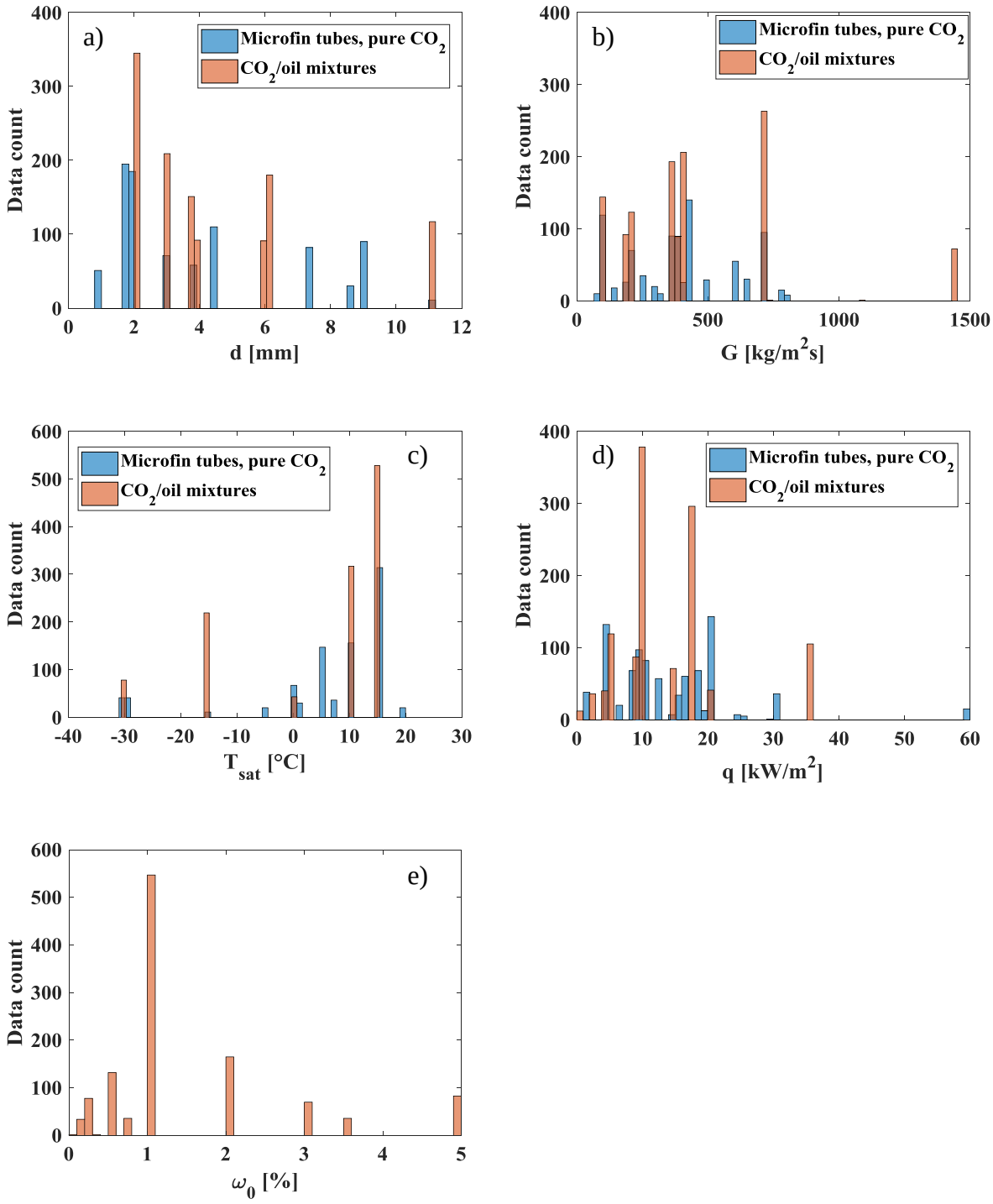

Figure 13 Distribution of data points for flow boiling of CO_2 in enhanced tubes and in smooth tubes with the presence of lubricating oil, related to: (a) internal diameter; (b) mass flux; (c) saturation temperature; (d) imposed heat flux; (e) nominal oil mass fraction

The experimental Nusselt numbers of the two databases are compared with both nucleate and convective Nusselt, respectively from Equations (1) and (7) in Figure 14a-b, as previously presented for conventional geometries and pure carbon dioxide. As already pointed out, the heat transfer coefficients in microfin tubes can be considerably higher than those obtained in an

equivalent smooth geometry, mainly due to the increased heat transfer surface and also to a higher turbulence of the liquid in the tube with a subsequent enhancement of the heat transfer convection efficiency. As a consequence, the experimental Nusselts calculated in enhanced tubes (black circular markers) are significantly underestimated by considering either only convection or only nucleation, and therefore specific heat transfer prediction methods should instead be employed. In case of CO_2/oil mixtures, the experimental Nusselt numbers (red diamond markers in Figure 14) are lower than the corresponding values calculated for only convective and only nucleative Nusselt values, implying a non-negligible penalization with respect to the flow boiling in smooth tubes with pure carbon dioxide. In fact, the two-phase heat transfer coefficient is altered by the presence of lubricant that affects both convective and nucleate boiling contributions, as also shown in Figure 12. From one side, bubble nucleation and growth tend to be suppressed due to the simultaneous increase of the saturation temperature and the surface tension of the liquid mixture. However, as suggested by Thome [91], this effect can be partially compensated with foaming, that increases the nucleation phenomenon. As regards the convective contribution, although the increase of the surface tension might delay the onset of dryout (which occurs at low vapor qualities in case of CO_2) through an increased wettability, the higher viscosity of the mixture liquid phase greatly penalizes the flow velocity and thus convective heat transfer.

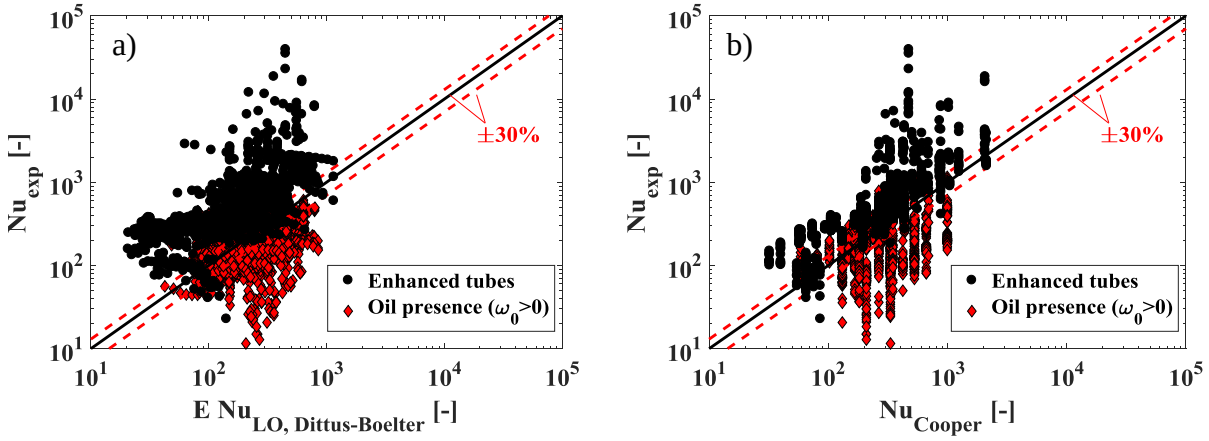

Figure 14 Experimental versus predicted Nusselt numbers, for enhanced tubes and CO_2/oil mixtures. Comparison with convective (a) and nucleate (b) boiling contribution

5.2 Assessment of methods: enhanced tubes

To the best of our knowledge, the only flow boiling heat transfer prediction method explicitly developed for microfin tubes (with 0° helix angle) and carbon dioxide as working fluid is that of Wu et al. [44]. Before the dryout region, the heat transfer coefficient was calculated using the same

expression of Yoon et al. [26], by introducing the fin height H_{fin} as supplementary geometrical parameter, as shown in Equation (11):

$$h_{Wu,x<x_{cr}} = \left[C_1 Bo^{C_2} \left(\frac{P_{sat} d}{\sigma} \right)^{C_3} + C_4 \left(1/X_{tt} \right)^{C_5} \left(\frac{G H_{fin}}{\mu_L} \right)^{C_6} \right] \cdot Re_{LO}^{C_7} Pr_L^{C_8} \left(\frac{\delta}{H_{fin}} \right)^{C_9} \cdot h_L \tag{11}$$

where Re_{LO} is the Reynolds number evaluated for liquid-only flow, h_L is the liquid Dittus-Boelter heat transfer coefficient and δ is the liquid film thickness that must be calculated in the hypothesis of symmetric annular flow (Equation (4)), by employing the void fraction from Rohuani and Axelsson [70] expression. The nine coefficients from C_1 to C_9 were fitted by the experimental data, obtaining, respectively: 0.0077, 2.1, 1.1, 25, 0.41, -1.3, 0.82, 0.45 and -0.11. In the post-dryout region the heat transfer coefficient was instead correlated to the dry angle and the wet and vapor heat transfer coefficients values, as shown in the following Equation (12):

$$h_{Wu,x>x_{cr}} = \frac{\theta_{dry} h_V + \left(2\pi - \theta_{dry} \right) h_{wet}}{2\pi} \tag{12}$$

where h_V is the Dittus-Boelter vapor heat transfer coefficient and the dry angle is a function of the vapor Reynolds, Boiling and Bond numbers:

$$\frac{\theta_{dry}}{2\pi} = D_1 Re_L^{D_2} Bo^{D_3} Bd^{D_4} \tag{13}$$

The recommended values for the four coefficients from D_1 to D_4 are 0.37, 0.29, 0.23 and -0.46. The heat transfer coefficient of the wet portion must be evaluated with Equation (11), in which the liquid film thickness δ is calculated with the following expression:

$$\delta = \frac{d}{2} \left(1 - \sqrt{1 - \frac{1-\alpha}{1 - \frac{\theta_{dry}}{2\pi}}} \right) \tag{14}$$

Finally, the dryout vapor quality was correlated to the liquid Reynolds, Boiling and Bond numbers and to the ratios of liquid and vapor density and viscosity as follows:

$$x_{cr} = E_1 Re_L^{E_2} Bo^{E_3} Bd^{E_4} \left(\frac{\rho_V}{\rho_L} \right)^{E_5} \left(\frac{\mu_L}{\mu_V} \right)^{E_6} \tag{15}$$

The fitted coefficients from E_1 to E_6 were, respectively: 1.3, -0.24, -0.11, 0.00095, 1.1 and 1.1. This correlation was entirely calibrated on the multi-minichannel microfin tube tested by the authors [44] and was intended to cover mass fluxes from 100 to 600 kg/m^{2}s, heat fluxes from 1.67 to 8.33 kW/m^2 and saturation temperatures from 1 to 15 °C.

The agreement between this correlation and the entire database for enhanced tubes is shown in Figure 15a. Although this prediction method includes the effect of the enhanced channel characteristics through the fin height, it largely fails to capture the experimental data (with a calculated *MAE* of 163%) and works quite well only for the authors' own database, as shown in Figure 15b, in which 92% of the data are predicted within an error band of ±50%.

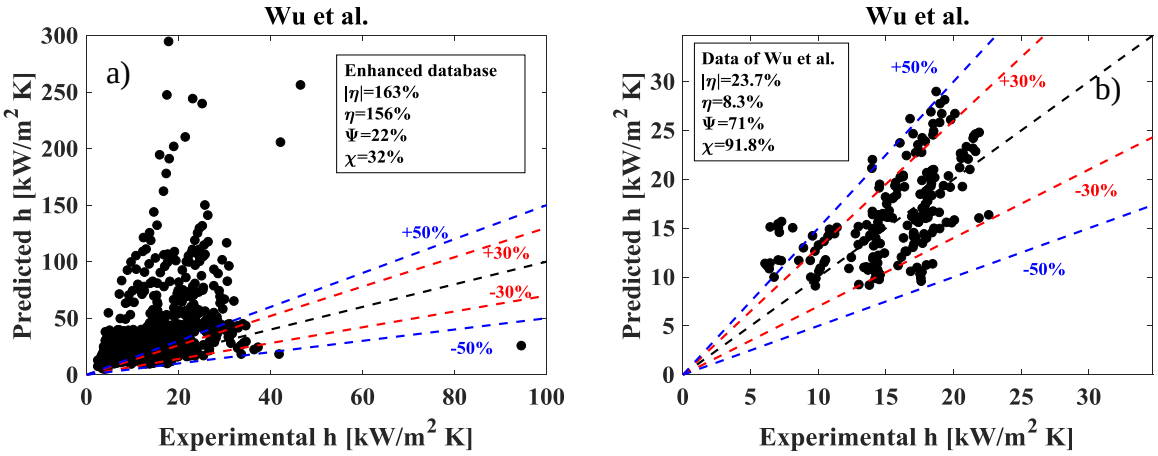

Figure 15 Experimental versus predicted heat transfer coefficients for enhanced surfaces. Correlation of Wu et al. **[44]** applied to: (a) All the collected data for enhanced surfaces. (b) Wu et al. **[44]** database

5.3 Assessment of methods: oil effect

Four different flow boiling heat transfer coefficient correlations developed for CO_2/PAG oil mixtures in smooth tubes are considered for this review. Most of the methods use a typical flow boiling structure, such as either a superposition or an asymptotic model, with an adjustment of the nucleate boiling suppression factor by considering the oil properties and and/or its concentration in the evaporating flow. A summary of the mathematical expressions of the four prediction methods is given in Table 6.

Aiyoshizawa et al. [92] proposed a typical superposition model in which the convection enhancement and the boiling suppression factors were calibrated on the experimental data of Dang et al. [62] for carbon dioxide and PAG oil. The simplicity of this method consists in the use of the pure CO_2 physical properties, whereas the presence of lubricant is taken into account only with the normal oil normal boiling point temperature $T_{b,oil}$.

Gao et al. [93] developed a flow boiling heat transfer coefficient prediction method for oil/CO_2 mixures based on their own experimental data for carbon dioxide and PAG oil. The same equations of Cheng et al. [66] [36] were employed for their asymptotic model, except for the additional suppression factor related to the vapor quality.

Katsuta et al. [57] employed a superposition model in which the nucleate boiling contribution was additionally penalized by the factor Φ depending on the nominal oil mass fraction.

Finally, Li et al. [94] developed an asymptotic method for flow boiling of carbon dioxide with entrained PAG oil for smooth horizontal tubes in the pre-dryout region. The thermodynamic properties labeled with the subscript *m* refer to the oil/refrigerant mixture. For their evaluation, a comprehensive set of equations can be found in the original references [94].

Table 6 Mathematical expressions of the flow boiling heat transfer prediction methods for carbon dioxide and lubricants mixtures in smooth tubes

Author	Equations	Range of validity
Aiyoshizawa et al. [92]	$h = Eh_L + Sh_{nb}$, liquid heat transfer coefficient with Dittus-Boelter equation $h_{nb} = 207\left(\frac{qD_b}{\lambda_L T_b}\right)^{0.745}\left(\frac{\rho_V}{\rho_L}\right)^{0.581}\mathrm{Pr}_L^{0.533}\frac{\lambda_L}{D_b}$ $D_b = 0.51\left[\frac{2\sigma}{g(\rho_L-\rho_V)}\right]^{0.5}$ $E = 0.8 + 0.5\left(1/X_{tt}\right)^{1.2}$ $S = \frac{1}{6+\left(\mathrm{Re}_{tp}\cdot 10^{-4}\right)^3}$ $\mathrm{Re}_{tp} = \mathrm{Re}_L \cdot E$	$2 \le d \le 6\ mm$ $360 \le G \le 1440\ kg\ m^{-2}s^{-1}$ $4.5 \le q \le 36\ kW\ m^{-2}$ $T_{sat} = 15\ °C$ $PAG\ oil;\ \omega_0 \le 5.0\%$
Gao et al. [93]	Same equations of the Cheng et al. [66] [36] model, with an additional suppression factor $h = \left[\left(S'h_{nb}\right)^3 + h_{cb}^3\right]^{1/3}$ $S' = S\cdot(-0.5x + 0.35)$ for $x \le 0.7$ $S' = 0$ for $x \le 0.7$.	$d = 3\ mm$ $190 \le G \le 1100\ kg\ m^{-2}s^{-1}$ $10 \le q \le 20\ kW\ m^{-2}$ $T_{sat} = 10\ °C$ $PAG\ oil;\ \omega_0 \le 0.57\%$
Katsuta et al. [57]	$h = Eh_L + Sh_{nb}\Phi$ $E = 1 + 0.258\left(1/X_{tt}\right)^{0.886} + 92.32\left(\frac{\rho_V}{\rho_L}\right)^3\left(1/X_{tt}\right)^{0.9}$ $S = \ln\left(2.332\cdot\frac{Bo^{0.518}Bd^{1.27}Fr^{0.964}}{\mathrm{Re}_{tp}^{0.834}}\right)$, with Re_{tp} taken from Aiyoshizawa et al. [92] $\Phi = \frac{1}{1+\omega_{oil}^{0.698}Bo^{0.207}Bd^{0.912}}$	$d = 3\ mm$ $G = 400\ kg\ m^{-2}s^{-1}$ $5 \le q \le 15\ kW\ m^{-2}$ $0 \le T_{sat} \le 10\ °C$ $PAG\ oil;\ \omega_0 \le 3.5\%$

Li et al. [94]	$h = \left[\left(Sh_{nb} \right)^3 + Eh_m^3 \right]^{1/3}$, nucleate boiling heat transfer coefficient from Forster and Zuber [77] and h_m from Dittus-Boelter equation. Both of them must be calculated with the properties of the CO_2/oil mixture, as recommended in [94] $E = 1$ for $X_{tt} \geq 10$ $E = 2.55 \cdot \left(0.413 + {}^{1}\!/\!_{X_{tt}} \right)^{1.05}$ for $X_{tt} < 10$ $S = S_{oil} \cdot \frac{1}{0.9 + \frac{0.4\left(\left(E^{1.25} \cdot Re_m \right) \cdot 10^{-3} \right)^{0.3}}{\left(Bo \cdot 10^3 \right)^{0.23}}}$ $S_{oil} = -\frac{\omega_{oil,x}}{2\ln\left(1 - \omega_{oil,x}\right)}$ $\omega_{oil,x} = \frac{\omega_0}{1 - x}$, local oil concentration $Re_m = \frac{G\left(1 - x\right)d}{\mu_m}$, with Re_m as the oil/CO_2 mixture Reynolds number.	$2 \leq d \leq 6\ mm$ $360 \leq G \leq 1440\ kg\ m^{-2}s^{-1}$ $4.5 \leq q \leq 36\ kW\ m^{-2}$ $T_{sat} = 15\ °C$ $PAG\ oil;\ \omega_0 \leq 5.0\%$

The assessment of the CO_2/oil flow boiling prediction methods with the individual works and for the entire collected database is provided in Table 7. The calculated errors are quite high in any case, but the correlations of Aiyoshizawa et al. [92] and of Gao et al. [93] provide a discrete agreement with almost all the single databases, with overall calculated MAE of 73.7% and 63.2%, respectively. The graphical comparison of these two prediction methods is shown in Figure 16a-b, in which it is clear the large scatter for a considerable amount of points, especially those obtained for higher nominal oil mass fractions (defined by the color bar). The correlation of Katsuta et al. [57] works particularly well with the data collected from Pehlivanoglu et al. [59] and from Kim et al. [60] [83], together with the authors' own database, but largely fails in the other cases. The remaining prediction method of Li et al. [94] greatly overestimates all the experimental heat transfer coefficients, providing an overall relative error of +165%.

Table 7 Assessment of the CO_2 flow boiling heat transfer coefficient prediction methods for smooth tubes in the presence of oil (along the columns), compared to the individual experimental database (along the rows)

Author	**Aiyoshizawa et al.** [92]	**Gao et al.** [93]	**Katsuta et al.** [57]	**Li et al.** [94]
Gao et al. [56]	|η|=108 η=94.5 ψ=71 χ=71	|η|=45.4 η=32.2 ψ=73 χ=82	|η|=300 η=300 ψ=4.4 χ=4.4	|η|=202 η=191 ψ=0 χ=8.9
Katsuta et al. [57]	|η|=48.2 η=15.7 ψ=54 χ=79	|η|=130 η=130 ψ=0 χ=8.5	|η|=39.8 η=8.2 ψ=62 χ=77	|η|=162 η=160 ψ=17 χ=26
Pehlivanoglu et al. [59]	|η|=54.2 η=-50.5 ψ=17 χ=34	|η|=54.4 η=-52.2 ψ=21 χ=33	|η|=31.1 η=-30.4 ψ=34 χ=99	|η|=70 η=36.8 ψ=34 χ=53
Kim et al. [60] [83]	|η|=54.6 η=-50 ψ=9.4 χ=26	|η|=56.9 η=-55.8 ψ=6 χ=33	|η|=24.1 η=-24.1 ψ=65.8 χ=97	|η|=61 η=34.1 ψ=39.3 χ=62
Ono et al. [61]	|η|=76.1 η=58.7 ψ=68 χ=78	|η|=43.6 η=11.9 ψ=62 χ=80	|η|=226 η=226 ψ=0 χ=0	|η|=170 η=155 ψ=4.6 χ=8
Dang et al. [62]	|η|=89 η=85.6 ψ=68 χ=70	|η|=82 η=75.7 ψ=43 χ=55	|η|=312 η=312 ψ=0 χ=0	|η|=242 η=242 ψ=0.4 χ=2.3
Overall database with oil	**|η|=73.7** **η=38.8** **ψ=52.4** **χ=62.4**	**|η|=63.2** **η=24.2** **ψ=42.2** **χ=56.9**	**|η|=204** **η=190** **ψ=11.9** **χ=26.1**	**|η|=176** **η=165** **ψ=12.2** **χ=20.1**

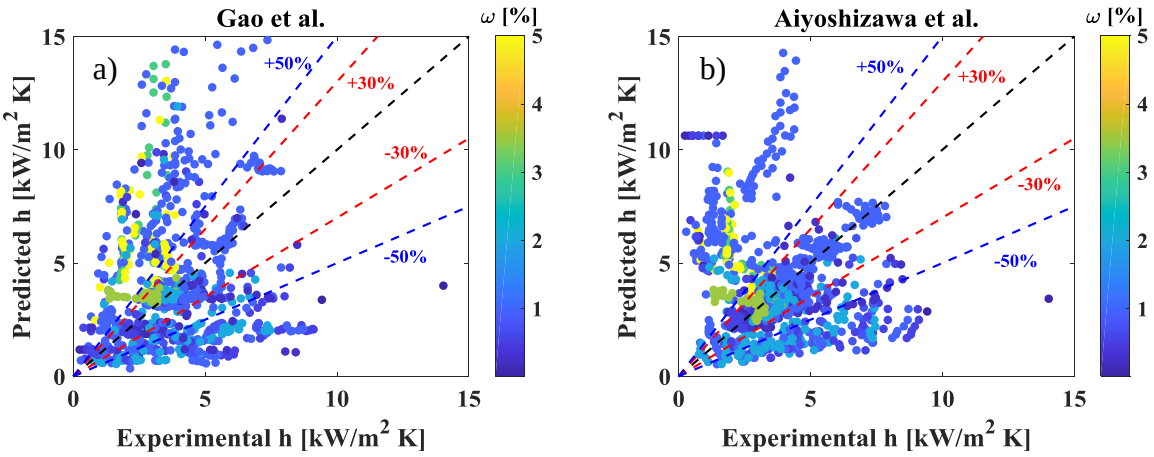

Figure 16 Experimental versus predicted heat transfer coefficients with the presence of oil for the entire database presented in **Table 5**. The color bar refers to the initial oil mass fraction. (a) Correlation of Gao et al. **[93]**. (b) Correlation of Aiyoshizawa et al. **[92]**

6. Conclusions

A comprehensive review of flow boiling heat transfer of carbon dioxide has been presented in this paper. The review addresses flow boiling experimental studies in smooth and enhanced tubes with pure CO_2 and CO_2/lubricant mixtures, collecting more than 7000 heat transfer coefficient data points and analyzing the main trends with operating conditions. The experimental Nusselt numbers are compared to the nucleate and convective contribution for each data set and the assessment of existing prediction methods explicitly developed for carbon dioxide is finally carried out. The main outcomes of this review are summarized as follows:

- By considering the macro-to-micro scale transition criterion of Kew and Cornwell [21], there are no significant differences in the flow boiling behavior of pure CO_2 in smooth tubes. Pure convective (*h* increasing only with vapor quality and mass flux) and pure nucleative (*h* increasing only with saturation temperature and heat flux) trends can in fact be both found either for small and conventional channels, depending on the operating conditions explored.
- Data from smooth tubes and pure CO_2 are segregated into different flow patterns according to the flow pattern map of Cheng et al. [66]. Points belonging to bubbly, intermittent, stratified-wavy and slug flow are fairly fitted by considering a pure nucleate boiling contribution (*MAE* = 51%), expressed by the Cooper [67] correlation for pool boiling heat transfer. Annular flow data are instead not fairly predicted with either only convection or only nucleation heat transfer

- Among the twelve CO_2-related heat transfer coefficient prediction methods available in literature for smooth tubes, the superposition model of Oh et al. [30] best predicts data belonging to bubbly, slug, intermittent and stratified-wavy flow, with a calculated *MAE* of 33.3%. In case of annular flow regime, the best agreement is found with the method of Hihara and Tanaka [72], with a calculated *MAE* of 27%. Although carrying higher errors, the flow pattern based methods of Thome and El-Hajal [35] and of Pettersen [42] best fit the dryout and mist flow experimental heat transfer coefficients, respectively. By considering the entire database, the Pettersen [42] method provides the lowest *MAE* of 46%, with similar accuracy for both micro and macro scale.
- Generally, with respect to smooth tubes at the same operating conditions, the two-phase heat transfer coefficients in microfin tubes are considerably higher. It was observed that the increased turbulence generated by the microfin structure is able to drive the liquid phase in the grooves, thus anticipating the appearance of the annular flow regime, providing at the same time a more convective behavior and a delayed dryout occurrence. The only available prediction method of Wu et al. [44] strongly overestimates the collected database for enhanced tubes, with an overall *MAE* of 163%.
- The presence of lubricant negatively affects both the convective and nucleate boiling heat transfer contributions of carbon dioxide, with a significant suppression of the bubble nucleation and an increased flow viscosity. On the other hand, it was observed that the higher surface tension of the mixture increases the stability of the liquid film and may delay the onset of dryout. Among the four CO_2/oil flow boiling heat transfer prediction methods, the correlations of Aiyoshizawa et al. [92] and of Gao et al. [93] provide the best agreement, even if the deviations are quite high (*MAE* of 73.7% and 63.2%, respectively).

Acknowledgements

Luca Viscito received a grant at Federico II University funded by “Ministero dell’Istruzione dell’Università e della Ricerca”, via the project PRIN2015 “Clean Heating and Cooling Technologies For An Energy Efficient Smart Grid”, which is gratefully acknowledged.

References

[1] M.H. Kim, J. Pettersen, C.W. Bullard, Fundamental process and system design issues in CO2 vapor compression systems, Progress in Energy and Combustion Science 30 (2004), 119-174.

[2] R. Thevenot, A history of refrigeration throughout the world, Paris: IIR; 1979 (Fidler JC, Trans.).

[3] B. Donaldson, B. Nagengast, Heat and cold: mastering the great indoors. Atlanta, GA: ASHRAE; 1994.

[4] Kohlendioxid. Besondereheiten und Einsatzchancen als Kaltemittel. Statusbericht des Deutschen Kalte-und Klimatechnischen Vereins, Nr 20. DKV, Stuttgart, 1998.

[5] G. Lorentzen, The use of natural refrigerants: a complete solution to the CFC/HCFC predicament, Int. J. Refrigeration 18(3) (1995), 190-197.

[6] R. Mastrullo, A.W. Mauro, J.R. Thome, G.P. Vanoli, L. Viscito, Flow boiling of Carbon Dioxide at Low to Medium Reduced pressures - Part 1. Carbon Dioxide Thermodynamic and Thermophysical Properties. Encyclopedia of Two-Phase Heat Transfer and Flow IV, Modeling Methodologies, Boiling of CO2, and micro-two-phase cooling (2018), World Scientific, doi:10.1142/9789813234420_0001.

[7] A. Bredesen, A. Hafner, J. Pettersen, K. Aflekt, Heat transfer and pressure drop for in-tube evaporation of CO2, Int. Conf. Heat Transfer Issues in Natural Refrigerants, College Park, MD (1997), 1-15.

[8] J.R. Thome, G. Ribatski, State-of-the-art of two-phase flow and flow boiling heat transfer and pressure drop of CO2 in macro- and micro-channels, Int. J. Refrigeration 28 (2005) 1149-1168.

[9] P. D'Agaro, M.A. Coppola, G. Cortella, Field tests, model validation and performance of a CO2 commercial refrigeration plant integrated with HVAC system, Int. J. Refrigeration 100 (2019) 380-391.

[10] R. Llopis, L.Nebot-Andrés, D. Sànchez, J. Catalàn-Gil, R. Cabello, Subcooling methods for CO2 refrigeration cycles: a review, Int. J. Refrigeration 93 (2018) 85-107.

[11] G. Mitsopoulos, E. Syngounas, D. Tsimpoukis, E. Bellos, C. Tzivanidis, S. Anagnostatos, Annual performance of a supermarket refrigeration system using different configurations with CO2 refrigerant, Energy Conversion and Management: X 1 (2019), 100006.

[12] D. Sànchez, R. Llopis, R. Cabello, J. Catalàn-Gil, L. Nebot-Andrés, Conversion of a direct to an indirect commercial (HFC134a/CO2) cascade refrigeration system: Energy impact analysis, Int. J. Refrigeration 73 (2017) 183-199.

[13] C. Sanz-Kock, R. Llopis, D. Sànchez, R. Cabello, E. Torrella, Experimental evaluation of a R134a/CO2 cascade refrigeration plant, Appl. Th. Engineering 73 (1) (2014) 41-50.

[14] S. Taslimi Taleghani, M. Sorin, S. Poncet, H. Nesreddine, Performance investigation of a two-phase transcritical CO2 ejector heat pump system, Energy Conversion and Management 185 (2019) 442-454.

[15] Y. Zhu, C. Li, F. Zhang, P.X. Jiang, Comprehensive experimental study on a transcritical CO2 ejector-expansion refrigeration system, Energy Conversion and Management 151 (2017) 98-

106.

[16] J. Chen, S. Jarall, H. Havtun, B. Palm, A review on versatile ejector applications in refrigeration systems, Renewable and Sustainable Energy reviews 49 (2015) 67-90.

[17] C.C. Wang, K.Y. Chi, Heat transfer and friction characteristics of fin-and-tube heat exchangers, part I: new experimental data, Int. J. Heat Mass Transfer 43 (2000) 2681-2691.

[18] C.C. Wang, K.Y. Chi, C.J. Chang, Heat transfer and friction characteristics of plain fin-and-tube heat exchangers, part II: Correlation, Int. J. Heat Mass Transfer 43 (2000) 2693-2700.

[19] S.S. Mehendale, A.M. Jacobi, R.K. Shah, Fluid flow and heat transfer at micro-and meso-scale with application to heat exchanger design, Applied Mechanics Reviews 53(7) (2000) 175-193.

[20] S.G. Kandlikar, W.J. Grande, Evolution of microchannel flow passages - Thermohydraulic performance and fabrication technology, Heat Transfer Engineering 24(1) (2003) 3-17.

[21] P. Kew, K. Cornwell, Correlations for the prediction of boiling heat transfer in small-diameter channels, Appl Therm Eng 17 (1997) 705-715.

[22] R. Yun, Y. Kim, M.S. Kim, Y. Choi, Boiling heat transfer and dryout phenomenon of CO2 in a horizontal smooth tube, Int. J. Heat Mass Transfer 46 (2003) 2353-2361.

[23] K. Gungor, R. Winterton, A general correlation for flow boiling in tubes and annuli, Int. J. Heat Mass trans. 29 (1986) 351-358.

[24] R. Yun, Y. Kim, M.S. Kim, Convective boiling heat transfer characteristics of CO2 in microchannels, Int. J. Heat Mass Transfer 48 (2005) 235-242.

[25] R. Yun, Y. Kim, Post-dryout heat transfer characteristics in horizontal mini-tubes and a prediction method for flow boiling of CO2, Int. J. Refrigeration 32 (2009) 1085-1091.

[26] S.H. Yoon, E.S. Cho, Y.W. Hwang, M.S. Kim, K. Min, Y. Kim, Characteristics of evaporative heat transfer and pressure drop of carbon dioxide and correlation development, Int. J. Refrigeration 27 (2004) 111-119.

[27] X. Zhao, P.K. Bansal, Flow boiling heat transfer characteristics of CO2 at low temperatures, Int. J. Refrigeration 30 (2007) 937-945.

[28] K.I. Choi, A.S. Pamitran, J.T. Oh, Two-phase flow heat transfer of CO2 vaporization in smooth horizontal minichannels, Int. J. Refrigeration 30 (2007) 767-777.

[29] K.I. Choi, A.S. Pamitran, C.Y. Oh, J.T. Oh, Boiling heat transfer of R-22, R-134a and CO2 in horizontal smooth minichannels, Int. J. Refrigeration 30 (2007) 1336-1346.

[30] J.T. Oh, A.S. Pamitran, K.I. Choi, P. Hrnjak, Experimental investigation on two-phase flow boiling heat transfer of five refrigerants in horizontal small tubes of 0.5, 1.5 and 3.0 mm inner diameters, Int. J. Heat Mass Transfer 54 (2011) 2080-2088.

[31] E. Hihara, C. Dang, Coiling heat transfer of carbon dioxide in horizontal tubes, Proceedings of HT2007 2007 ASME-JSME Thermal Engineering Summer Heat Transfer Conference, July 8-12 (2007), Vancouver, British Columbia, Canada.

[32] C.Y. Park, P.S. Hrnjak, CO2 and R410A flow boiling heat transfer, pressure drop, and flow pattern at low temperatures in a horizontal smooth tube, Int. J. Refrigeration 30 (2007) 166-178.

[33] H.K. Oh, H.G. Ku, G.S. Roh, C.H. Son, S.J. Park, Flow boiling heat transfer characteristics of carbon dioxide in a horizontal tube, Appl. Therm. Engineering 28 (2008) 1022-1030.

[34] H.K. Oh, C.H. Son, Flow boiling heat transfer and pressure drop characteristics of CO2 in horizontal tube of 4.57-mm inner diameter, Appl. Th. Engineering 31 (2011) 163-172.

[35] J. R. Thome, J. El Hajal, Flow boiling heat transfer to carbon dioxide: general prediction method, Int. J. Refrigeration 27 (2004) 294-301.

[36] L. Cheng, G. Ribatski, J.R. Thome, New prediction methods for CO2 evaporation inside tubes: Part II - An updated general flow boiling heat transfer model based on flow patterns, Int. J. Heat Mass Transfer 51 (2008) 125-135.

[37] R. Mastrullo, A.W. Mauro, A. Rosato, G.P. Vanoli, Carbon dioxide local heat transfer coefficients during flow boiling in a horizontal circular smooth tube, Int. J. Heat Mass Transfer 52 (2009) 4184-4194.

[38] R. Mastrullo, A.W. Mauro, J.R. Thome, G.P. Vanoli, CO2 and R410A: two-phase flow visualizations and flow boiling measurements at medium (0.50) reduced pressure, Appl. Th. Engineering 49 (2012) 2-8.

[39] S. Grauso, R. Mastrullo, A.W. Mauro, G.P. Vanoli, Flow boiling of R410A and CO2 from low to medium reduced pressures in macro channels: Experiments and assessment of prediction methods, Int J Heat Mass Trans 56 (2013) 107-118.

[40] Y. Zhu, X. Wu, Z. Wei, Heat transfer characteristics and correlation for CO2/propane mixtures flow evaporation in smooth mini tube, Appl. Th. Engineering 81 (2015) 253-261.

[41] J. Pettersen, R. Rieberer, S.T. Munkejord, Heat transfer and pressure drop characteristics of evaporating carbon dioxide in microchannel tubes, IIF-IIR - Commission B1, B2, E1, and E2 - Purdue University, USA - 2000.

[42] J. Pettersen, Flow vaporization of CO2 in microchannel tubes, Exp. Th. Fluid Science 28 (2004) 111-121.

[43] S. Jeong, D. Park, Evaporative heat transfer of CO2 in a smooth and a micro-grooved miniature channel tube, Heat Transfer Engineering 30(7) (2009) 582-589.

[44] X. Wu, Y. Zhu, Y. Tang, New experimental data of CO2 flow boiling in mini tube with micro fins of zero helix angle, Int. J. Refrigeration 59 (2015) 281-294.

[45] J.L. Gasche, Carbon dioxide evaporation n a single microchannel, J. of the Brazilian Society of Mech. Science & Eng. 28 (2006) 69-83.

[46] D. Gorenflo, Pool Boiling, VDI Heat Atlas, VDI Verlag, Dusseldorf (1993).

[47] M. Ducoulombier, S. Colasson, J. Bonjour, P. Haberschill, Carbon dioxide flow boiling in a single microchannel - Part II: Heat transfer, Exp. Th. Fluid Sc. 35 (2011) 591-611.

[48] J. Linlin, L. Jianhua, Z. Liang, L. Qi, X. Xiaojin, Characteristics of heat transfer for CO2 flow boiling at low temperature in mini-channel, Int. J. Heat Mass Transfer 108 (2017) 2120-2129.

[49] Z. Liang, J. Linlin, L. Jianhua, Z. Yue, Investigation of flow boiling heat transfer characteristics of CO2 in horizontal mini-tube, Int. J. Thermal Sciences 138 (2017) 109-115.

[50] M. Ozawa, T. Ami, H. Umekawa, R. Matsumoto, T. Hara, Forced flow boiling of carbon dioxide in horizontal mini-channel, Int. J. Thermal Sciences 50 (2011) 296-308.

[51] M. Ozawa, T. Ami, I. Ishihara, H. Umekawa, R. Matsumoto, Y. Tanaka, T. Yamamoto, Y. Ueda, Flow pattern and boiling heat transfer of CO2 in horizontal small-bore tubes, Int. J. Multiphase Flow 35 (2009) 699-709.

[52] A.E. Schael, M. Kind, Flow pattern and heat transfer characteristics during flow boiling of CO2 in a horizontal microfin tube and comparison with smooth tube data, Int. J. Refrigeration 28 (2005) 1186-1195.

[53] J.M. Cho, M.S. Kim, Experimental studies on the evaporative heat transfer and pressure drop of CO2 in smooth and micro-fin tubes of the diameters of 5 and 9.52 mm, Int. J. Refrigeration 30 (2007) 986-994.

[54] J.M. Cho, Y.J. Kim, M.S. Kim, Experimental studies on the characteristics of evaporative heat transfer and pressure drop of CO2/propane mixtures in horizontal and vertical smooth and micro-fin tubes, Int. J. Refrigeration 33 (2010) 170-179.

[55] N.B. Chien, P.Q. Vu, K.I. Choi, J.T. Oh, Boiling heat transfer of R32, CO2 and R290 inside horizontal minichannel, Energy Procedia 105 (2017) 4822-4827.

[56] L. Gao, T. Honda, S. Koyama, Experiments on flow boiling heat transfer of almost pure CO2 and CO2-oil mixtures in horizontal smooth and microfin tubes, HVAC&R Research 13 (3) (2007) 415-425.

[57] M. Katsuta, K. Okuma, T. Hirade, N. Miyachi, The effect of the lubricating oil fraction rate on the CO2 evaporating thermal and hydraulic characteristics, International Refrigeration and Air Conditioning Conference at Purdue, July 14-17, 2008.

[58] S. Grauso, R. Mastrullo, A.W. Mauro, G.P. Vanoli, CO2 and propane blends: Experiments and assessment of predictive methods for flow boiling in horizontal tubes, Int. J. Refrigeration 34 (2011) 1028-1039.

[59] N. Pehlivanoglu, S. Kim, P.S. Hrnjak, Effect of oil on heat transfer and pressure drop of R744 in 6.1 mm horizontal smooth tube, International Refrigeration and Air Conditioning Conference at Purdue, July 12-15, 2010.

[60] S. Kim, N. Pehlivanoglu, P.S. Hrnjak, R744 flow boiling heat transfer with and without oil at low temperatures in 11.2 mm horizontal smooth tube, International Refrigeration and Air Conditioning Conference at Purdue, July 12-15, 2010.

[61] T. Ono, L. Gao, T. Honda, Heat transfer and flow characteristics of flow boiling of CO2-oil mixtures in horizotnal smooth and micro-fin tubes, Heat Transfer - Asian Research 39 (3) (2010) 195-207.

[62] C. Dang, N. Haraguchi, T. Yamada, M. Li, E. Hihara, Effect of lubricating oil on flow boiling heat transfer of carbon dioxide, Int. J. Refrigeration 36 (2013) 136-144.

[63] J. Wu, T. Koettig, C. Franke, D. Helmer, T. Eisel, F. Haug, J. Bremer, Investigation of heat transfer and pressure drop of CO2 two-phase flow in a horizontal minichannel, Int. J. Heat Mass Transfer 54 (2011) 2154-2162.

[64] V.P. Carey, Liquid-vapor phase-change phenomena - An introduction to the thermophysics of vaporization and condensation processes in heat transfer equipment, Washington D.C.: Hemisphere Publishing Corporation, 1992.

[65] G. Lillo, R. Mastrullo, A.W. Mauro, L. Viscito, Flow boiling of R1233zd(E) in a horizontal tube: Experiments, assessment and correlation for asymmetric annular flow, Int. J. Heat Mass Transfer 129 (2019) 547-561.

[66] L. Cheng, G. Ribatski, J.M. Quiben, J.R. Thome, New prediction methods for CO2

evaporation inside tubes: Part I - A two-phase flow pattern map and a flow pattern based phenomenological model for two-phase flow frictional pressure drops, Int. J. Heat Mass Trans. 51 (2008) 111-124.

[67] M.K. Cooper, Saturated nucleate pool boiling: A simple correlation, First UK Natl. Heat Transfer Conf. 2 (1984) 785-793.

[68] F.W. Dittus, L.M.K. Boelter, Heat transfer in automobile radiators of the tubular type, Univ. Calif. Publ. Eng. 2 (1930) 443-461.

[69] D. Steiner, Heat transfer to boiling saturated liquids. In: Verein Deutscher Ingenieure (Ed.), VDI-Wärmeatlas (VDI Heat Atlas). VDI-Geseelschaft Verfahrenstechnik und Chemieingenieurswesen (GCV) 1993, Düsseldorf.

[70] Z. Rohuani, E. Axelsson, Calculation of volume void fraction in a subcooled and quality region. International Journal of Heat and Mass Transfer 17 (1970) 383-393..

[71] D. Mikielewicz, B. Jakubowska, Prediction of flow boiling heat transfer coefficient for carbon dioxide in minichannels and conventional channels, Archives of Thermodynamics 37(2) (2016) 89-106.

[72] E. Hihara, S. Tanaka, Boiling heat transfer of carbon dioxide in horizontal tubes, Preliminary Proceedings IIR at Purdue, 279-284.

[73] M.M. Shah, M.A. Siddiqui, A general correlation for heat transfer during dispersed-flow film boiling in tubes, Heat Transfer Engineering 21(4) (2000) 18-32.

[74] A.S. Kon'kov, Experimental study on the conditions under which heat exchange deteriorates when a steam-water mixture flows in heated tubes, Teploenergetika 13 (12) (1965) 77.

[75] S.Y. Ahmad, Fluid to fluid modeling of critical heat flux: a compensated distortion model, Int. J. Heat Mass Transfer 16 (1973) 641-662.

[76] Y. Hwang, B.H. Kim, R. Radermacher, Boiling heat transfer correlation of carbon dioxide, Int. Conference on Heat Transfer Issues in Natural Refrigerants, University of Maryland, USA, 1997, 81-95.

[77] H.K. Forster, N. Zuber, Dynamics of vapor bubbles and boiling heat transfer, AIChE Journal 1 (1955) 531-535.

[78] N. Kattan, J.R. Thome, D. Favrat, Flow boiling in horizontal tubes: Part 1 - development of a diabatic two-phase flow pattern map, J. Heat Transfer 120 (1998) 140-147..

[79] N. Kattan, J.R. Thome, D. Favrat, Flow boiling in horizontal tubes: Part 3 - Development of a new heat transfer model based on flow patterns, J. Heat Transfer 120 (1) (1998) 156-165..

[80] A.S. Pamitran, K.I. Choi, J.T. Oh, Nasruddin, Evaporation heat transfer coefficient in single circular small tubes for flow natural refrigerants of C3H8, NH3 and CO2, Int. J. Multiphase Flow 37 (2011) 794-801.

[81] C. Dang, N. Haraguchi, E. Hihara, Flow boiling heat transfer of carbon dioxide inside a small-sized microfin tube, Int. J. Refrigeration 33 (2010) 655-663.

[82] X. Zhao, P.K. Bansal, Flow boiling heat transfer analysis of new experimental data of CO2 in a micri-fin tube at -30 °C, Int. J. Thermal Sciences 59 (2012) 38-44.

[83] S. Kim, P.S. Hrnjak, Effect of oil on flow boiling heat transfer and flow patterns of CO2 in 11.2 mm horizontal smooth and enhanced tube, International Refrigeration and Air

Conditioning Conference at Purdue, July 16-19, 2012.

[84] C.J. Seeton, J. Fahl, D. Henderson, Solubility, viscosity, boundary lubrication and miscibility of CO2 in synthetic lubricants, Proc. 4th IIR-Gustav Lorentzen Conference on Natural Working Fluids at Purdue (2000) 417-424.

[85] A. Hauk, E. Weidner, Thermodynamic and fluid-dynamic properties of carbon dioxide with different lubricants in cooling circuits for automobile application, Ind. Chem. Res. 39 (2000) 4646-4651.

[86] C.C Wang, A. Hafner, C.S. Kuo, W.D. Hsieh, An overview of the effect of lubricant on the heat transfer performance on conventional refrigerants and natural refrigerant R-744, Ren. Sustain. Energy Rev. 16 (2012) 5071-5086.

[87] J.R. Thome, Comprehensive Thermodynamic approach to modeling refrigerant-lubricating oil mixtures, HVAC&R Res. (1995), 110-126.

[88] E.P. Bandarra Filho, L. Cheng, J.R. Thome, Flow boiling characteristics and flow pattern visualization of refrigerant/lubricant oil mixtures, Int. J. Refrigeration 32 (2009) 185-202.

[89] A. Yokozeki, Solubility correlation and phase behaviors of carbon dioxide and lubricant oil mixtures, Applied Energy 84 (2007) 159-175.

[90] M.A. Marcelino Neto, J.R. Barbosa Jr, Phase and volumetric behaviour of mixtures of carbon dioxide (R-744) and synthetic lubricant oils, The Journal of Supercritical Fluids 50 (2009) 6-12.

[91] J.R. Thome, Boiling of refrigerants: A state of the art review, Int J. Refrigeration 19 (1996) 435-457.

[92] K. Aiyoshizawa, T. Yamada, N. Haraguchi, C. Dang, E. Hihara, The influence of lubricating oil on boiling heat transfer characteristics of carbon dioxide in horizontal smooth tubes. In: Proceedings of the 43rd National Heat Transfer Symposium of Japan, Nagoya, Japan (2006), CD-G133.

[93] L. Gao, Y. Matsusaka, M. Sato, T. Honda, Correlations of evaporation heat transfer of CO2-PAG oil mixtures in a horizontal smooth tube. In: Proceedings of the 2008 JSRAE Annual Conference, October 20-23, 2008,Osaka, Japan, Japan Society of Refrigeration and Air Conditioning Engineers (2008) 279-282.

[94] M. Li, C. Dang, E. Hihara, Flow boiling heat transfer of carbon dioxide with PAG-type lubricating oil in pre-dryout region inside horizontal tube, Int. J. Refrigeration 41 (2014) 45-59.